A load-based approach for optimizing a packed-bed thermal store

Bruno Cárdenas*, Seamus D. Garvey
Department of Mechanical, Materials and Manufacturing Engineering, University of Nottingham, University Park, NG7 2RD, United Kingdom

Abstract

This paper presents a load-based optimization approach for improving the efficiency of a packed bed. The optimization is based on splitting the work-cycle of the thermal store into two frequency components: low and high. A packed bed is designed for each one of the two profiles. A packed bed can be customised much better for a duty-cycle that contains a narrow range of frequencies.
The case study presented considers a 24h working-cycle (12h charge / 12h discharge) with a 10 MW peak power and an exergy storage requirement of 33.3 MWh (76.3 MWh of heat). A packed bed was optimized for this duty-cycle using a one dimensional model that varies the aspect ratio and the rock size. This packed bed is the 'reference case' for the study. The aim of the load-based optimization is to create a two-bed system that achieves lower exergy losses than the reference case while keeping the overall storage capacity constant.
A sign-preserving filter is used as the signal-splitting tool. Numerous different work-cycle "splits" are explored. Results show that the exergy losses of the packed bed can be considerably reduced. The optimum work-cycle split considers a low-frequency packed bed that supplies 85% of the storage capacity and a high-frequency packed bed that provides the remaining 15%. The combined losses of the two packed beds are 644 kWh, which represents a reduction of 25.5 % in comparison to the exergy losses of the reference case. The study demonstrates that the "load-based optimization" allows replacing a packed bed with an equivalent but more efficient two-bed system at almost no additional cost.

Keywords
Sign-preserving filter; load optimization; thermal energy storage; compressed air energy storage; exergy efficiency; work-cycle frequency

Table of Contents

1. Introduction
1.1 Objective and justification
2. The signal-splitting tool: a sign preserving filter
3. Methodology
3.1 Creation of the work-profiles for the frequency optimization
3.2 Mathematical model for designing a packed bed
4.1 Analysis of the reference case
4.2 Results obtained for the low-frequency packed bed (B)
4.3 Results obtained for the high-frequency packed bed (C)
4.4 Overall results achieved by the load-based optimization
5. Concluding remarks
References

1. Introduction

Energy storage has received considerable attention in recent years from both, the industrial and academic communities. It is deemed as a feasible and economically attractive solution to the grid balancing problem caused by the variability in the output of renewable generation [1,2]. Besides being an enabler for the further penetration of renewables into the grid, energy storage technologies offer users the ability of carrying out energy arbitrage [3-4] and, provided it is a thermal solution, the possibility of recovering waste heat from industrial processes [5].

Several thermo-mechanical systems for bulk storage of energy have been proposed and widely studied [6]. These include compressed air energy storage (CAES) [7-9], liquid air energy storage (LAES) [10-12] and pumped heat energy storage (PHES) [13-15]. All of them are regarded as very promising technologies and considerable amounts of research and resources have been devoted towards improving their performance and cost-effectiveness.

One component that the above systems have in common—and is key to their operation—is a thermal store. Packed beds of rock are the most commonly used type of thermal storage in these systems due to a number of desirable features such as: high efficiencies attainable, low cost, simplicity, compatibility with different heat transfer fluids (HTF) and broad operating temperature range (120-1200 K). Packed beds can also be used in concentrated solar power (CSP) plants for storing solar heat at times of high irradiation and low demand prior to generating electricity or as stand-alone components for the recovery of industrial waste heat.

Nomenclature Table

Acronyms		δt	Duration of time step (s)
CAES	Compressed Air Energy Storage	δx	Height of an element of the geometry (m)
CSP	Concentrated Solar Power	ΔP	Pressure drop (Pa)
HTF	Heat Transfer Fluid	ΔT	Temperature difference between hot and cold ends of packed bed (K)
LAES	Liquid Air Energy Storage	D_P	Particle diameter (m)
PHES	Pumped Heat Energy Storage	ε	Void fraction
PPtS	Peak Power to Size ratio	f	Friction factor
RMS	Root Mean Square	h	Convection coefficient (W/m²·K)
RPtS	RMS Power to Size	k	Thermal conductivity (W/m·K)
VRE	Variable Renewable Energy	K_B	Capacity ratio of the signal split
Sub-indices		μ	Dynamic viscosity (Pa·s)
c	Container	M	Mass (kg)
g	Gas	Nu	Nusselt number
r	Rock	N_{runs}	Number of runs carried out by filter
Symbology		ρ	Density (kg/m³)
α	Aspect ratio	P	Pressure (Pa)
$\boldsymbol{A}$	Original working cycle	Pr	Prandtl number
A	Cross-sectional area (m²)	Q_a	Heat transferred by advection (J)
$\boldsymbol{B}$	Low-frequency part of working cycle	Q_{conv}	Heat transferred by convection (J)
B	Exergy content (MWh)	Q_K	Heat transferred by conduction (J)
B_{in}	Total exergy input during charge (MWh)	R	Specific gas constant (J/kg·K)
B_{l-Ex}	Exhaust exergy losses (MWh)	Re	Reynolds number
B_{l-HT}	Exergy losses due to heat transfer (MWh)	s_r	Surface area of rocks (m²)
B_{l-PD}	Exergy losses due to pressure drops (MWh)	*Size*	Energy storage capacity (MWh)
B_{l-SD}	Exergy losses due to self-discharge (MWh)	t	Time (s)
B_{out}	Total exergy output during discharge (MWh)	T	Temperature (K)
$\boldsymbol{C}$	High-frequency part of working cycle	v_g	Superficial velocity of flow (m/s)
C_P	Specific heat capacity (J/kg·K)	W_{max}	Max. wavelet width used by filter

A packed bed consists of a container filled with a heat storage material, such as rock pebbles or small ceramic particles. A hot HTF (air, steam, oil) is pumped through the top of the container to charge the packed bed. As the hot HTF flows downwards, heat is transferred to the rocks. Energy is stored in the rocks as a consequence of their temperature change. To discharge the packed bed, the direction of the flow is reversed. A cold HTF enters the container through the bottom side and extracts heat from the rocks as it flows upwards. A thermal front (known as a thermocline) moves down and up the packed bed as it is charged or discharged. Packed beds can be either pressurized or non-pressurized. The latter configuration is commonly preferred due to the lower cost of the container; however in most cases a heat exchanger will be required somewhere else in the system.

The bulk energy storage systems mentioned above (CAES, LAES, PTES) depend on exergy-efficient and cost effective thermal stores; therefore, special attention should be paid to their design. A vast amount of research has been devoted to develop and validate analytical models for characterizing the behaviour of packed beds and for simulating their performance under different work cycles [16-27]. Additionally, numerous authors have carried out parametric studies aimed at understanding the effect that different design and operational parameters (particle size, void fraction, mass flow rates, charging/discharging rates, materials used, etc.) have on the performance of the thermal storage units [28-37].

Notwithstanding, there is still an ample area of opportunity for improving the current designs of packed beds. More efficient or less expensive packed beds will lead to more cost-effective large-scale energy storage systems. This paper build on work carried out by the University of Nottingham [38-41]. The study incorporates the numerical models previously developed into a novel optimization approach that focuses on the frequency of the duty-cycle of a packed bed with aims at reducing its roundtrip exergy losses.

1.1 Objective and justification

The objective of this work is to demonstrate that it is possible—in some cases—to achieve a reduction in the total exergy losses of a packed bed by splitting its work cycle into

two (or more) profiles based on frequency ranges. Each one of the smaller work-cycles created is handled by an independent packed bed that has beeen expressly designed for it. The design of a packed bed can be much better tailored for a work cycle that contains a narrower range of frequencies. If a packed bed is intended for operating under a high-frequency work cycle, it will need very small rocks to maximize the surface area and meet the rapid heat transfer requirements of the cycle. However this causes an increased pressure drop across the height of the packed bed, which represents an operational cost. On the other hand if the packed bed will operate under a low-frequency cycle, larger rocks can be used to minimize the pumping load because a fast-response capability is not imperative in this case.

An example that illustrates the effect that the frequency of the work-cycle has on the performance of a packed bed is given below. Cárdenas et al. [39] carried out a parametric study in which a packed bed was optimized for the work-cycle shown in Figure 1a. The optimum packed bed designed (called "packed bed *X*") had roundtrip exergy losses of 0.589 MWh. These losses are composed in the following way: 188.7 kWh are owed to heat transfer, 166.8 kWh owed to pressure drops, 201 kWh owed to self- discharge and 33.1 kWh are exhaust losses. A better explanation of the meaning of each type of exergy loss is given in section 4.1. The packed bed *X* achieved an exergy efficiency of 98.24% while working under the duty-cycle shown in Figure 1a.

Figure 1b shows a signal that is based on the sine wave from Figure 1a but has a considerable amount of noise. This peculiar profile was contrived with the specific objective of having a signal that is equivalent in many ways to the pure sine wave of Figure 1a (peak power, RMS power and energy content) but that at the same time has an obvious mix of different frequencies. Table 1 provides some of the key parameters of both work profiles.

The noisy signal from Figure 1b was used as the working profile for packed bed *X* (which is optimized for Fig.1a). The performance observed in this situation is much worse. The roundtrip exergy losses of packed bed *X* increased by ~48% reaching a total of 0.873 MWh. The losses are broken down as follows: 421.2 kWh due to heat transfer, 144.9 kWh due to pressure drops, 306.6 kWh due to self-discharge and 0.227 kWh owed to exhaust losses.

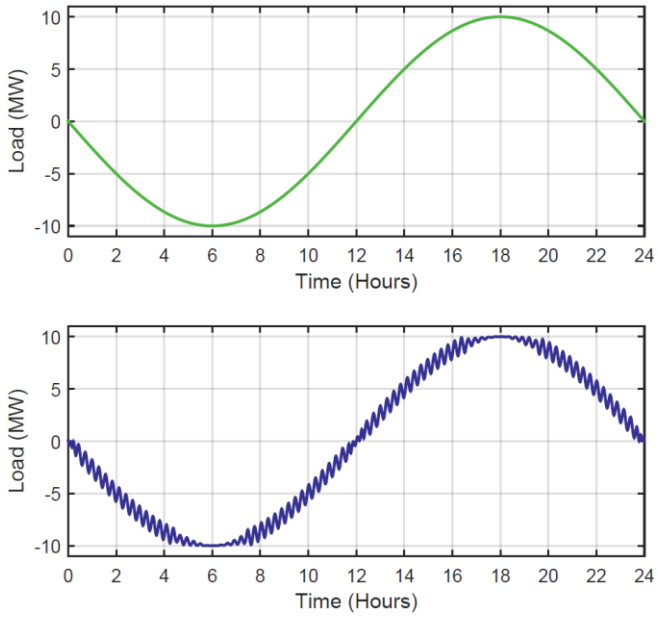

Figure 1. Two equivalent signals used as work-profiles: a) pure sine, b) sine with added noise.

Table 1. Comparison of the two signals shown in Figure 1.

Parameter	Profile Fig. 1a	Profile Fig. 1b
Peak Power (MW)	10	10
Mean Power (Half Cycle)	6.3662	6.3610
RMS Power (MW)	7.071	7.079
Energy Content (MWh)	76.39	76.332
Peak Power to Energy Ratio	0.1309	0.1310
RMS Power to Energy Ratio	0.0926	0.0928

Figure 2 shows the temperature profiles developed by packed bed *X* while operating under the two different working cycles. A sharper thermal front is seen when the packed bed operates under the noisy signal (Fig 1b). Owing to this (among other factors), the temperature of the cold end at the end of the charging cycle (12^{th} hour) is not much higher than its nominal value. This helps to minimize exhaust losses.

It can also be seen that when the packed bed operates under the noisy signal, the temperature of its hot end at the end of the discharge period (0^{th} hour) is ~540K, which is much lower than the nominal temperature of 823.15 K. This large temperature difference causes substantial heat transfer losses during the subsequent charging phase because air at 823.15K will ingress the packed bed through the hot end and will come in contact with rocks at a much lower temperature, which destroys exergy.

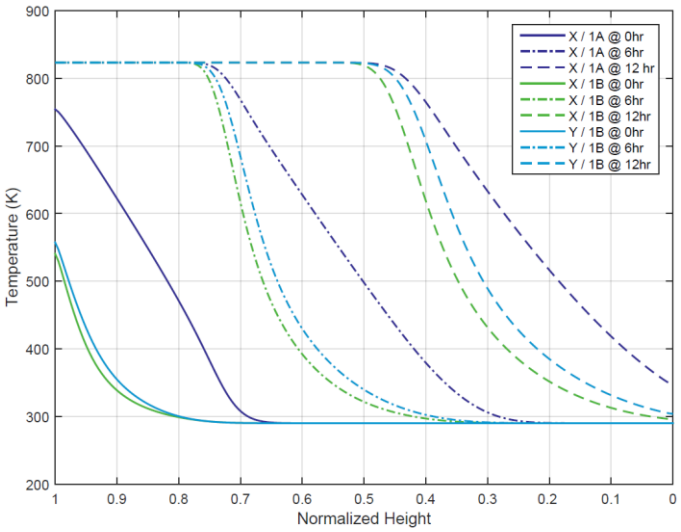

Figure 2. Temperature profiles of 2 different packed beds (X and Y) working under different work-cycles. Blue: Packed bed X working under sine wave. Green: Packed bed X working under noisy wave. Cyan: Packed bed Y working under noisy wave

Using the same model from [39], a packed bed was designed and optimized for the 'noisy' signal shown in Figure 1b. This packed will be called *Y*. The design of packed bed *Y* is somewhat different to the design of packed bed *X*. The aspect ratio went from 0.6 to 0.7 and the particle size jumped from 4 to 6.5 mm.

Packed bed *Y* has roundtrip exergy losses of 0.865 MWh when operating under the work-cycle of Figure 1b. The exergy losses consist of: 526.6 kWh of exergy loss due to heat transfer, 117.2 kWh due to pressure drops, 1.54 kWh due to exhaust losses and 220.4 kWh due to self- discharge. Exergy losses due to pressure drops are smaller in comparison to those of packed bed *X* because the particle size increased. However, using larger rocks reduces the overall heart transfer area and causes increased heat transfer losses. Packed bed *Y* experiences reduced self-discharge losses thanks to the combined effect of using larger rocks and having a greater separation between the hot and cold ends (owing to a larger aspect ratio). Figure 2 shows the thermal front of packed bed *Y* at different times different during the work-cycle.

The losses of packed bed *X* when subjected to the noisy profile (0.873 MWh) are higher than when the pure sinusoidal cycle is passed through it (0.589 MWh); despite the fact that the two work-cycles are very similar to each other. This suggests that a mix of different frequencies will affect the performance of the packed bed even if the power of the work-cycle stays the same.

Furthermore, the losses of packed bed *Y*, which has been optimized for working under the noisy profile (0.865 MWh), are only slightly smaller than the losses seen by packed bed *X* when working under the same profile (0.873 MWh). This suggests that if a packed bed is optimized for a work-cycle that contains a mix of different frequencies, its design will suffer from the compromises that the optimization algorithm has to make in order to balance heat transfer characteristics and pressure drops. Table 2 summarizes the results of the simulations carried out with packed beds *X* and *Y*.

Table 2. Comparison between some design and performance parameters of two different packed beds *X* and *Y* operating under equivalent work-cycles.

	Packed Bed X	**Packed Bed X**	**Packed Bed Y**
Aspect Ratio	0.6	0.6	0.7
Rock Diameter (mm)	4	4	6.5
Optimized for work-cycle	Fig. 1a	Fig. 1a	Fig. 1b
Used for work-cycle	Fig. 1a	Fig. 1b	Fig. 1b
Heat input (MWh)	76.39	76.332	76.332
Total exergy input (MWh)	33.559	33.511	33.483
Exergy input due to heat (MWh)	33.392	33.366	33.366
Exergy input due to pressure (MWh)	0.167	0.145	0.117
Exergy recovered (MWh)	32.97	32.638	32.618
Exergy losses due to heat transfer (kWh)	188.7	421.2	526.6
Exergy losses due to pressure drops (kWh)	166.8	144.9	117.2
Exhaust exergy losses (kWh)	33.1	0.227	1.54
Exergy losses due to self-discharge (kWh)	201	306.6	220.4
Total exergy losses (MWh)	0.589	0.873	0.865
Exergy efficiency (%)	98.24	97.39	97.41

The foregoing leads to the premise that the efficiency of a packed bed could be improved if the work-cycle ($\boldsymbol{A}$), which contains a mix of different frequencies, was split into two smaller profiles ($\boldsymbol{B}$ and $\boldsymbol{C}$) with a narrower frequency range. A packed bed is then designed and optimized for each of these two frequency components. This research paper aims to prove that the above is indeed possible.

2. The signal-splitting tool: a sign preserving filter

There are a number of different methods for splitting a signal $\boldsymbol{A}$ into two or more frequency components. One of the most commonly used techniques is the Fourier analysis. Figure 3a shows the decomposition of a signal $\boldsymbol{A}$ using this technique. The low-frequency components are grouped in the signal $\boldsymbol{B}$ while signal $\boldsymbol{C}$ contains the high-frequency spectrum. It can be seen that the signs of the two outputs differ from each other

in many points in time (e.g. t=12). This phenomenon is called 'counter-flow'. In many applications counter-flow is not a problem but in some others—such as the optimization of a packed bed—it is highly undesirable.

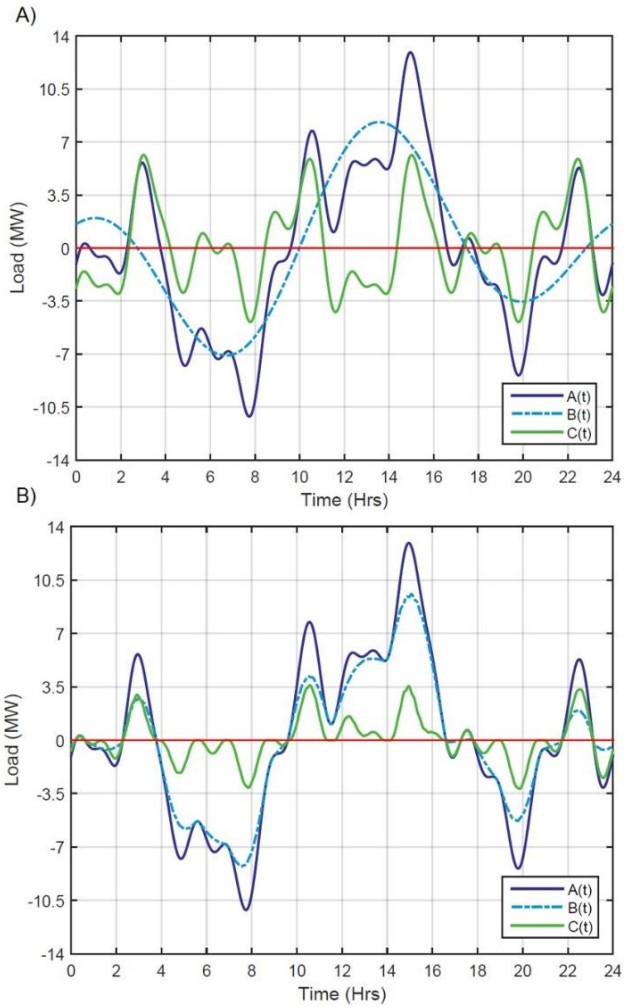

Figure 3. Examples of signal decompositions using: (a) Fourier analysis and (b) Sign-Preserving filter.

The packed bed is in discharge mode when $\boldsymbol{A}$ is positive and in charging mode when $\boldsymbol{A}$ is negative. The two smaller packed beds used for the signals $\boldsymbol{B}$ and $\boldsymbol{C}$ work in the same way. These two packed beds are expected to work in parallel to replicate the operation of the single packed bed working under $\boldsymbol{A}$. However, there are many instances (e.g. t=4 and t=12) in which one packed bed is effectively charging the other. Having counter-flow in the system means that instead of working together, packed beds $\boldsymbol{B}$ and $\boldsymbol{C}$ counteract each other to produce the desired final effect (replicating $\boldsymbol{A}$). Passing heat unnecessarily from one store to the other increases the overall exergy losses owing to the stacking up of inefficiencies.

In addition to that, the counter-flow phenomenon causes the total storage capacity of the system to increase with respect to the storage capacity of packed bed $\boldsymbol{A}$. The storage capacity to service a certain duty is determined by integrating the work-cycle ($\boldsymbol{A}$), which is typically expressed as a power signal. The result of the integration is an energy profile that shows how the energy accumulated in the packed bed increases or decreases throughout the work-cycle's length. The difference between the highest and lowest values of this energy profile indicates the minimum storage capacity ($size$) that the packed bed needs in order to handle the duty.

$$Size = \max_{0\le t\le T}\left(\int A(t)dt\right) - \min_{0\le t\le T}\left(\int A(t)dt\right) \quad (1)$$

For example, a packed bed sized for the work-cycle $\boldsymbol{A}$ (Fig.3a) needs to have an energy storage capacity of 40.783 MWh. The storage capacities of the packed beds for $\boldsymbol{B}$ and $\boldsymbol{C}$ are determined to be 38.79 MWh and 8.14 MWh, respectively. It is clear that the existing counter-flow caused an increase of ~15% in the total storage capacity. A larger storage capacity requires a larger mass of rocks and consequently represents a higher cost. It has been demonstrated that the efficiency of a packed bed will improve if the mass of rock increases for the same storage duty [39]. Nevertheless, enlarging the thermal store to improve its efficiency is the equivalent of "*paying more to make something better*". The 'load-based optimization' method presented in this paper seeks to improve the efficiency of a packed bed without increasing its overall size nor its cost.

None of the existing signal processing tools are capable of splitting a signal (work-cycle) without creating some counter-flow. Therefore they are not suitable for this application. Cárdenas et al. [41] developed a "Sign-Preserving-filter" that allows separating a discrete time signal $\boldsymbol{A}$ into two components ($\boldsymbol{B}$ and $\boldsymbol{C}$) without generating the aforementioned counter-flow problem. $\boldsymbol{B}$ is a mostly low-frequency signal and $\boldsymbol{C}$ is a mostly high-frequency signal. The key features of the filter are that the sum of $\boldsymbol{B}$ + $\boldsymbol{C}$ replicates $\boldsymbol{A}$ exactly and that the signs of $\boldsymbol{B}$ and $\boldsymbol{C}$ are equal to the sign of $\boldsymbol{A}$ at every time t, as Eqs. (2) and (3) show.

$$A(t) = B(t) + C(t) \quad (2)$$

$$sgn\big(A(t)\big) = sgn\big(B(t)\big) = sgn(C(t)) \quad (3)$$

At the start of the filtering process, the signal $\boldsymbol{B}$ is initialized as a copy of $\boldsymbol{A}$ while signal $\boldsymbol{C}$ is set to zero. The filter works by

passing wavelets of different widths throughout the length of signal $\boldsymbol{B}$. With every pass, some amount of 'non-smoothness' is subtracted from $\boldsymbol{B}$ and stored in $\boldsymbol{C}$. The operation of the filter is controlled by two user-defined parameters: the maximum wavelet width (w_{max}) and the number of runs (n_{runs}). One run consists of two passes with every odd wavelet contained in the range from $w = 3$ to $w = w_{max}$. Several runs (n_{runs}) can be carried out to produce a smoother low-frequency signal $\boldsymbol{B}$.

Figure 3b shows an example of a decomposition carried out with the sign preserving filter. It can easily be seen that the two output signals have the same sign as the original work-profile at all times. In this case, a packed bed sized for the low-frequency signal $\boldsymbol{B}$ would have a storage capacity of 33.607 MWh the packed bed sized for the high-frequency signal $\boldsymbol{C}$ would only need a capacity of 7.257 MWh. Their combined storage capacity adds to 40.864 MWh, which is an almost negligible increase (<0.2%) with respect to the capacity of the original packed bed $\boldsymbol{A}$.

The sign-preserving filter is used in this research work as the tool for creating the different work-profiles that need to be explored. The mechanics of the operation of the filter will not be addressed in any more detail in this paper. A comprehensive explanation of the underlying algorithm can be found in [41]. The filter has previously been used in a similar "load-based" optimization work, which was aimed at designing a hybrid battery pack for an electric vehicle [42].

3. Methodology

The work profile ($\boldsymbol{A}$) used for this study is the noisy sine wave previously shown in Figure 1b. The work-profile $\boldsymbol{A}$ can be split into a low-frequency component ($\boldsymbol{B}$) and a high-frequency component ($\boldsymbol{C}$) in many different ways using the sign preserving filter. The optimization algorithm will try to find the 'split' of $\boldsymbol{A}$ for which the combined exergy losses of the packed beds optimized for the profiles $\boldsymbol{B}$ and $\boldsymbol{C}$ are minimized. If the optimization is successful, these losses will be smaller than the losses of the packed bed optimized for $\boldsymbol{A}$.

The process followed to find the optimum 'split' is shown graphically by Figure 4. The starting point is to design and optimize a packed bed for the work-cycle $\boldsymbol{A}$ using the model from [39]. The performance achieved by packed bed $\boldsymbol{A}$ sets the target for the 'load-optimization'.

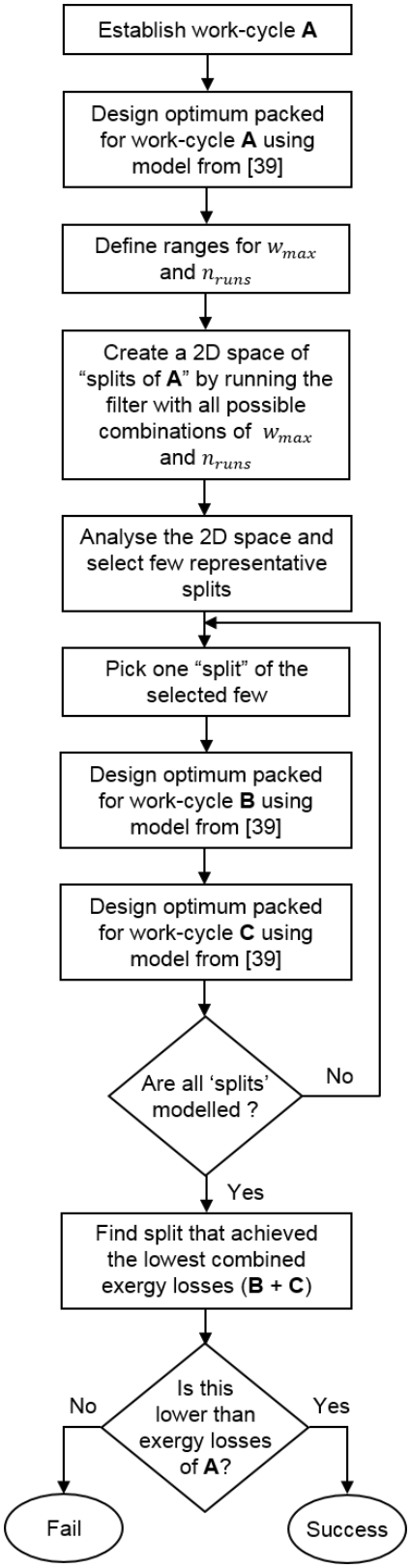

Figure 4. Algorithm followed by the 'load-based' approach to optimize a packed bed for a given work cycle $\boldsymbol{A}$

The signal $\boldsymbol{A}$ is split using the sign-preserving filter. A two-dimensional search space that contains all the different possible ways to split the working profile is created with the two control parameters of the filter: w_{max} and n_{runs}. Ideally all the 'splits' in the 2D search space would be explored; however the optimization of a packed bed for a given working profile is a computationally expensive task. Therefore optimizing a packed bed for the two signals in each of the *n* different splits contained in the 2D space would be unfeasible.

The 2D search space is reduced by selecting a few representative splits; subsection 3.1 describes in detail the strategy followed. The signals $\boldsymbol{B}$ and $\boldsymbol{C}$ from the selected 'splits' are used as work-profiles and a packed bed is designed and optimized for each one of them. The signal $\boldsymbol{B}$ of one 'split' is fed into a mathematical model that optimizes a packed bed for it. The process is repeated to optimize a packed bed for signal $\boldsymbol{C}$. The combined exergy losses of packed beds $\boldsymbol{B}$ and $\boldsymbol{C}$ constitute the total exergy losses for that specific split of $\boldsymbol{A}$.

The abovementioned numerical simulation process is repeated until all the packed beds for all the 'splits' of the work-cycle $\boldsymbol{A}$ have been modelled. The split that attains the lowest combined exergy losses ($\boldsymbol{B}$+$\boldsymbol{C}$) is the optimum split. These losses should be lower than the exergy losses of the reference case, otherwise the optimization has failed. It is important to highlight that the success of the 'load-based' optimization depends largely on the shape of the original work-profile (amount and type of noise contained); therefore not every work-profile can be optimized with the proposed approach.

3.1 Creation of the work-profiles for the frequency optimization

A two-dimensional search space is created by carrying out filtering operations on the reference profile $\boldsymbol{A}$ with all the possible combinations of the two parameters of the sign-preserving filter. The range defined for w_{max} spans from 3 to 151 points (odd values only) while n_{runs} goes from 1 to 100 runs. With these values 7500 different splits of $\boldsymbol{A}$ are created. Although the ranges for both control variables may seem arbitrarily defined, the space created does contain the optimum solution—as it will be demonstrated.

The search space can be reduced by expressing it in terms of a 'capacity ratio (K_B)' The capacity ratio is defined as the ratio of the storage capacity requirement of signal $\boldsymbol{B}$ with respect to that of signal $\boldsymbol{A}$, as Eq. (4) shows. In this way for example, it is possible to indicate that a split created with a w_{max}=55 and n_{runs}=33 has a K_B of 0.8, which means that packed bed $\boldsymbol{B}$ will store 80% of the total energy while packed bed $\boldsymbol{C}$ will store the remaining 20%.

$$K_B = Size\ (\boldsymbol{B})/Size\ (\boldsymbol{A}) \quad (4)$$

The first step to reduce the two-dimensional search space is to divide the range of possible values of K_B ($0.5 \leq K_B \leq 1$) into equally spaced intervals. Subsequently, the space is scanned to identify all the splits that fall within a range of ±1.5% of each one of the nominal values of K_B defined. The tolerance used is rather flexible but care must be taken to avoid overlap between ranges.

The above generates several groups of splits that still cover a large area of the two-dimensional space. For example, there are 261 different splits that have a capacity ratio in the range $K_B = 0.8 \pm 1.5\%$ and 112 that fall in the range $K_B = 0.6 \pm 1.5\%$. Each group contains a different amount of splits out of which one has to be selected.

The RMS-Power-to-Size (*RPtS)* ratio of the high-frequency signal $\boldsymbol{C}$ is used as the criterion to choose one split from each group. The split that contains the signal $\boldsymbol{C}$ with the lowest *RPtS* ratio is selected as the representative split for that nominal K_B. The *RPtS* ratio is an important parameter to consider because it has a strong influence on the performance of the packed bed. A small energy storage requirement ($size$) translates into reduced packed bed's dimensions (height and diameter). The higher the charging/discharging power is, the greater the air flow rate will be. Pumping air at fast rate through a container with a small cross-section causes a loss of exergy.

Table 3 shows the parameters of the different splits selected for each one of the nominal values of K_B. Figure 5 shows the signals $\boldsymbol{B}$ and $\boldsymbol{C}$ of each one of the splits selected for the different capacity ratios. These signals will be used as work-profiles and a packed bed will be designed and optimized for each one of them.

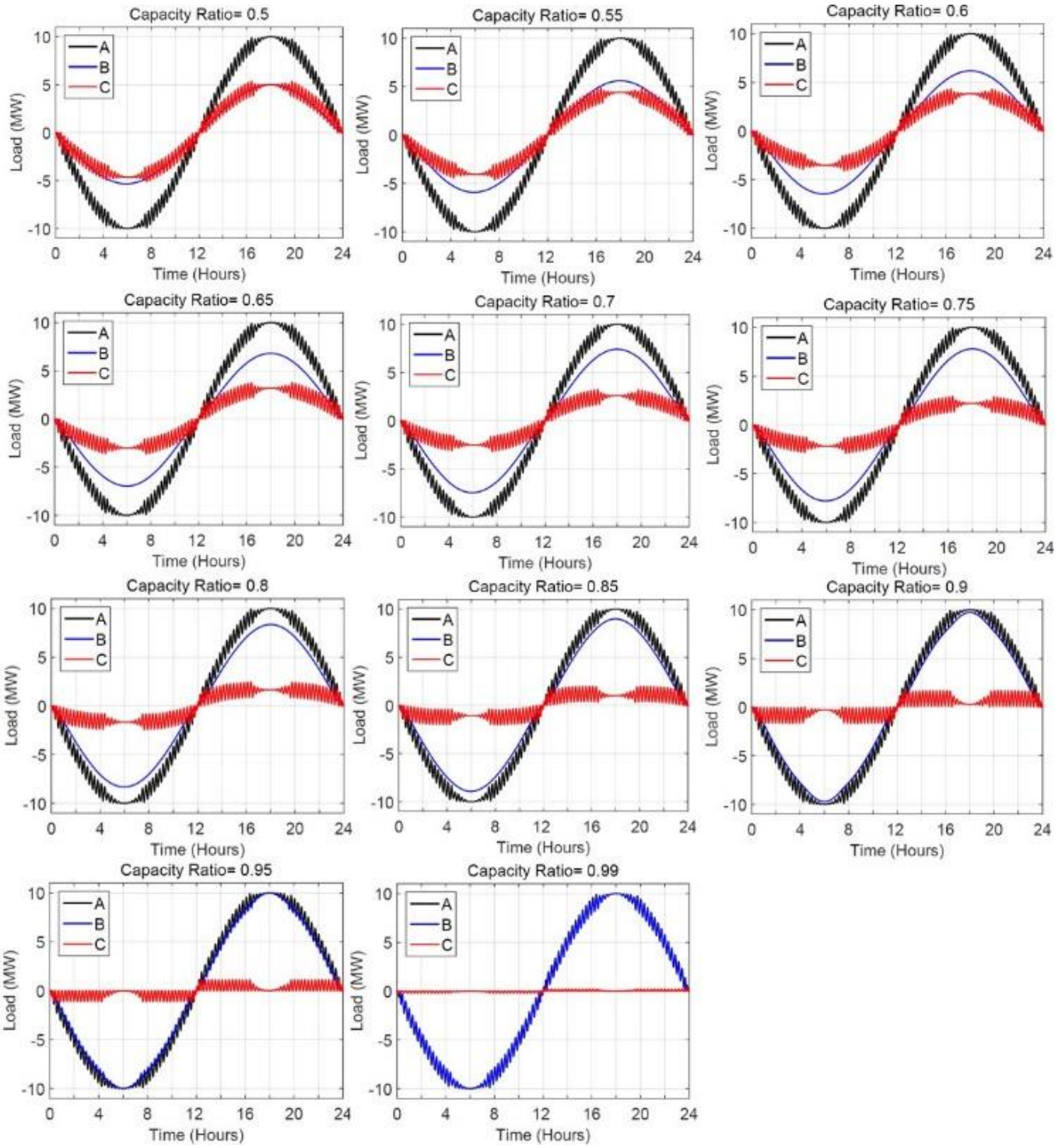

Figure 5. Comparison of signals (work-cycles) $\boldsymbol{B}$ and $\boldsymbol{C}$ for the different capacity ratios K_B

It is not possible to know whether a value of K_B is good or not without having passed the two signals through the mathematical model and assessed the performance achieved by the two corresponding packed beds. An educated guess—based on results from [42]—is that the optimum split will have a K_B larger than 0.7. It is reasonable to expect the packed bed in charge of the low-frequency part of the load to have a much larger storage capacity than the packed bed assigned to the high-frequency portion.

It is important to highlight that if a different strategy for reducing the search space was used, the final result would not differ much from what has been obtained in this study.

Table 3. Signal parameters of the selected 'split' for each nominal value of K_B

K_B Nominal	No. of Splits in range	Parameters of Split (Selected out of the group)				
		W_{max}	N_{runs}	K_B (Real)	RPtS Signal B	RPtS Signal C
0.99	2	3	83	0.9902	0.0930	0.1324
0.95	134	7	84	0.9359	0.0943	0.1158
0.9	977	27	54	0.8865	0.0953	0.1032
0.85	433	45	54	0.8373	0.0951	0.0934
0.8	261	51	67	0.7881	0.0949	0.0913
0.75	192	53	87	0.7415	0.0947	0.0909
0.7	152	55	96	0.7094	0.0946	0.0910
0.65	130	63	85	0.6591	0.0944	0.0913
0.6	112	107	26	0.6079	0.0942	0.0916
0.55	98	107	32	0.5559	0.0941	0.0919
0.5	86	105	41	0.5016	0.0939	0.0921

3.2 Mathematical model for designing a packed bed

This section of the paper provides a general overview of the mathematical model used to design and optimize a packed bed for a given work-cycle. The model was developed for a previous study and a more detailed explanation can be found in [39].

The first step of the modelling/optimization process is to analyse the work-cycle and determine the storage capacity required (see Eq. (1)). This dictates how big the packed bed will be. The total mass of rock (m_r) that is needed is calculated by means of Eq. (5), where *Size* is the amount of heat to be stored, C_{pr} is the specific heat capacity of the rocks and ΔT is the temperature difference between the hot and cold ends of the packed bed. The factor of 1.5 is used to improve the efficiency of the store by increasing the mass of rock over the absolute minimum required. It was found in [39] that a ~50% of additional storage mass provides the best benefit from a techno-economic standpoint. The temperatures considered for the hot and cold ends of the packed bed are 823.15 and 290 K respectively. These are typical operating temperatures in CSP plants [43] and high temperature A-CAES systems [44].

$$m_r = (1.5 \cdot Size)/(C_{pr} \cdot \Delta T) \quad (5)$$

After determining the thermal storage mass, a number of geometric parameters such as the height, diameter and volume of the container are calculated. The simulation algorithm explores different combinations of aspect ratio (α) and particle size. The optimum design for the packed bed is the combination that attains the lowest roundtrip exergy losses.

It should be noted that the optimal design found is only an optimum for the particular work-cycle that was inputted into the model. To find the global optimum, the aforementioned process has to be carried out for all the different $\boldsymbol{B}$ and $\boldsymbol{C}$ profiles created from the different decompositions of $\boldsymbol{A}$ (see Fig.5).

The mathematical model is a one-dimensional transient model based on a discretised explicit scheme. The following features and/or assumptions are worth mentioning: 1) there is no temperature gradient in the radial direction, 2) the rock particles have a uniform temperature, 3) the packed bed has constant geometric properties and 4) radiative heat transfer and heat losses to the ambient are neglected.

The physical properties of the rocks are taken from experimental data reported by Hartlieb et al. [45]. In the temperature range defined, these rocks have an average thermal conductivity of 1.58 W/m-K and an average specific heat capacity of 0.958 kJ/kg-K. The physical properties for the air were taken from publications by Lemmon et al. [46, 47]. In the range of operating temperatures considered, the dynamic viscosity, thermal conductivity and specific heat capacity of air have average values of 9.115×10^{-4} mPa, 6.4 mW/m K and 1.043 kJ/kg-K, respectively.

The mathematical model simulates the charge or discharge of the packed bed as it marches through time. In every time-step, a mass flow of air ($\dot{m}_g$) corresponding to the load at that time is calculated. Based on it, the flow characteristics and pressure drops inside the packed bed can be determined.

The inlet pressure is calculated iteratively so that the air exits the packed bed at ambient pressure. In order to do so, a vector of initial guesses for the pressure (P) at each slice (or element) of the geometry is created. Based on this vector, the density (ρ_g) and velocity (v_g) of the air are calculated using Eqs. (6) and (7) respectively; in which R is the specific gas constant of the air, T_g is the temperature of the air at every slice and A_c is the cross-sectional area of the container.

$$\rho_g = P \cdot (R \cdot T_g)^{-1} \quad (6)$$

$$v_g = \dot{m}_g \cdot (\rho_g \cdot A_c)^{-1} \quad (7)$$

The Reynolds number (Re) for flow through a packed bed is given by Eq. (8), where μ is the dynamic viscosity of the air and D_p is the diameter of the rocks [48].

$$Re = \rho_g \cdot v_g \cdot D_p \cdot \mu^{-1} \quad (8)$$

The pressure drops (ΔP) across each of the slices of the geometry are calculated by means of Eq. (9) [49], where δx is the height of the slice, f is a friction factor [50] and ε is the void fraction. The friction factor is calculated through Eq. (10), which appropriate for the range of Re expected [51].

$$\Delta P = \frac{f \cdot \delta x \cdot \rho_g \cdot {v_g}^2 \cdot (1-\varepsilon)}{2 \cdot D_p \cdot \varepsilon^3} \quad (9)$$

$$f = 258\, Re^{-1} \cdot (1-\varepsilon) + 4.36 \cdot \left(\frac{0.66 Re}{1-\varepsilon}\right)^{-0.12} \quad (10)$$

The vector of pressures (P) is updated by adding the accumulated pressure drops. The iterations are repeated until the variation in the vector of pressures is negligible. After this, the convective heat transfer coefficient (h) can be calculated by means of Eq. (11) where k_g is the thermal conductivity of the air. The Nusselt (Nu) and Prandtl (Pr) numbers are given by Eqs. (12) and (13), respectively [52].

$$h = Nu \cdot k_g \cdot {D_P}^{-1} \quad (11)$$

$$Nu = 2.0 + 1.1 Pr^{0.33} \cdot [Re \cdot (1-\varepsilon)]^{0.6} \quad (12)$$

$$Pr = \mu \cdot C_{pg} \cdot {k_g}^{-1} \quad (13)$$

Thermal calculations are expressed in a discretised explicit form. The heat transfer model is based, as Figure 6 shows, on the energy balance of a slice i of the geometry. As it can be seen, the change of energy within the air is equal to the net heat flow by advection $(Q_{a-in} - Q_{a-out})$ plus the net heat flow by conduction $(Q_{k-in} - Q_{k-out})$ minus the heat transferred by convection to the rocks (Q_{conv}). This is mathematically expressed by Eq. (14), in which the indices i and j represent spatial and temporal positions, respectively.

$$\rho_g C_{pg} A_c \varepsilon \delta x \left(T_g^{(i,j+1)} - T_g^{(i,j)}\right) = \ldots \\ \ldots (Q_{a-in} - Q_{a-out}) + (Q_{k-in} - Q_{k-out}) - Q_{conv} \quad (14)$$

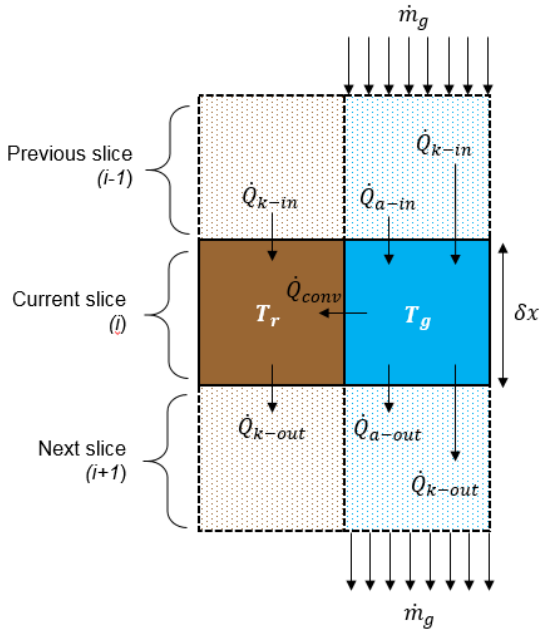

Figure 6. One-dimensional model of packed bed showing interactions between air (blue) and rock (brown) elements

The rate of change of the air temperature at time j can be expressed by Eq. (15):

$$\frac{\delta T_g}{\delta t} = \frac{Q_1 + Q_2 - Q_{conv}}{\rho_g C_{pg} A_c \varepsilon \delta x} \quad (15)$$

Where:

$$Q_1 = \frac{\dot{m}_g C_{pg}}{2}\left(T_g^{(i-1,j)} - T_g^{(i+1,j)}\right) \quad (16)$$

$$Q_2 = k_g A_g \left(\frac{T_g^{(i-1,j)} - 2T_g^{(i,j)} + T_g^{(i+1,j)}}{\delta x}\right) \quad (17)$$

In a similar fashion, the change of energy in the volume of rocks of a slice i can be calculated through Eq. (18):

$$m_r C_{pr}\left(T_r^{(i,j+1)} - T_r^{(i,j)}\right) = (Q_{k-in} - Q_{k-out}) + Q_{conv} \quad (18)$$

Rearranging Eq. (18) it is possible to obtain the rate of change of the temperature of the rocks, as Eq. (19) shows. This allows updating the temperature of the rocks after each time-step.

$$\frac{\delta T_r}{\delta t} = \frac{Q_3 + h s_r \left(T_g^{(i,j)} - T_r^{(i,j)}\right)}{m_r C_{pr}} \quad (19)$$

Where:

$$Q_3 = k_r A_r \left(\frac{T_r^{(i-1,j)} - 2T_r^{(i,j)} + T_r^{(i+1,j)}}{\delta x} \right) \quad (20)$$

The exergy input during the charge and the exergy output during the discharge are calculated by means of Eq. (21):

$$\dot{B}_g = \dot{m}_g \left[\int_{T_0}^{T} C_{pg} dT - T_0 \left(\int_{T_0}^{T} C_{Pg} \frac{dT}{T} - R \int_{P_0}^{P} \frac{dP}{P} \right) \right] \quad (21)$$

Four mechanisms of exergy loss are considered: 1) exergy losses due to heat transfer, 2) exhaust losses, 3) exergy losses due to pressure drops and 4) exergy losses due to self-discharge. The exergy losses due to pressure drops (B_{l-PD}) are calculated from the pressure drops in each slice of the geometry by means of Eq. (22):

$$B_{l-PD} = \sum_{i=1}^{x} -\dot{m}_g \cdot T_0 \cdot R \cdot ln \left(\frac{P^{(i+1,j)}}{P^{(i,j)}} \right) \quad (22)$$

As the packed bed charges up, hot air will start coming out of the cold end. This represents a loss of exergy and is referred to as "exhaust losses" (B_{l-Ex}). These losses can also be calculated through Eq. (21).

Exergy losses due to self-discharge (B_{l-SD}) are caused by the heat that is conducted down the temperature gradient inside the packed bed. These losses are always present. Self-discharge exergy losses are calculated by means of Eq. (23)

$$B_{l-SD} = \sum_{i=1}^{x-1} Q_{kg} \left(\frac{T_0}{T_g^{(i+1,j)}} - \frac{T_0}{T_g^{(i,j)}} \right) + Q_{kr} \left(\frac{T_0}{T_r^{(i+1,j)}} - \frac{T_0}{T_r^{(i,j)}} \right) \quad (23)$$

The exergy losses due to heat transfer (B_{l-HT}) refer to the losses caused by the convective heat transfer between air and rocks and the losses due to the advective heat transfer inherent to the flow of air. Heat transfer losses are in most cases the largest contributor to the total exergy losses and can be calculated through a simple exergy balance, as Eq. (24) shows:

$$B_{l-HT} = B_{in} - B_{out} - \Delta B_r - B_{l-PD} - B_{l-Ex} - B_{l-SD} \quad (24)$$

The mathematical model described above was implemented in MATLAB. In the program developed, the "time-stepping" is controlled by a built-in ordinary differential equation solver (ODE15s) which continuously adjusts the size of the time-steps in order to ensure that a certain user-defined tolerance is met. The solver estimates the solution (of one step) and the error of the integration using two Runge–Kutta methods with different local orders. If the error exceeds the tolerance defined, the step size is decreased until the error is below that tolerance. If the error is far below that tolerance, the step size is increased to save time. For this study we used a tolerance of $1x10^{-7}$. For the work-cycles considered in this work, the tolerance defined translates into time-steps much smaller than 0.1 second.

4.1 Analysis of the reference case

This section presents the design and optimization of the packed bed for the work-cycle ***A*** (see Fig. 1b). This work-cycle comprises a 12-hour charge followed by a 12-hour discharge. During the charge, 33.365 MWh of exergy are stored in the packed bed. This packed bed is the reference case or 'target' for the load-based optimization. The combined losses of packed beds ***B*** and ***C*** should be lower than those of packed bed ***A*.**

Figure 7 shows the behaviour of the total exergy losses of the packed bed with respect to the rock size. For simplicity, the plot only shows the curves for 4 aspect ratios. It can be seen that the effect of the rock size is more noticeable on packed beds with a small α. When a larger aspect ratio is used, the curves become flatter and a wider range of rock sizes yields a very similar level of losses.

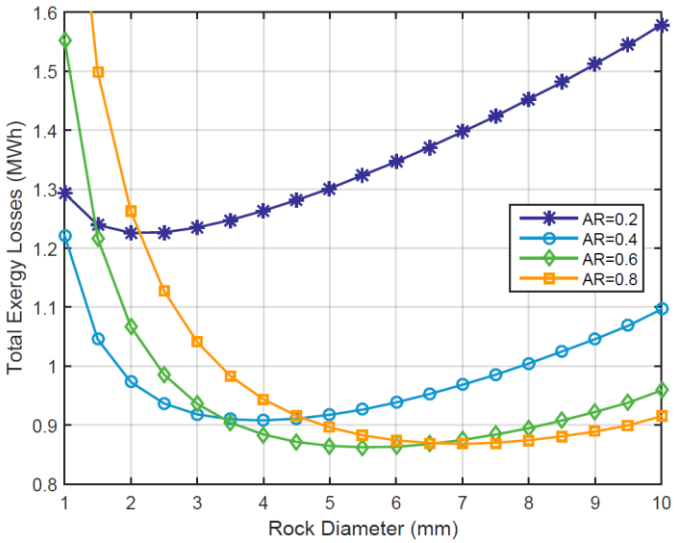

Figure 7. Effect of the aspect ratio and particle size on the total exergy losses of packed bed ***A***.

It can also be seen in Figure 7 that the optimum rock size increases with α. The cross-sectional area of the container grows as the aspect ratio reduces. This minimizes pressure drops and allows the optimizer to shift towards smaller particle sizes for improving heat transfer.

Figure 8 shows how the breakdown of the total exergy losses of packed bed $\boldsymbol{A}$ changes as α varies. The different designs presented in the figure consider the optimum rock size for each aspect ratio. It can be seen that for packed beds based on small aspect ratios, self-discharge losses are the main source of exergy loss. However, these losses stop being a problem as α starts to increase and pressure drops start to become critical.

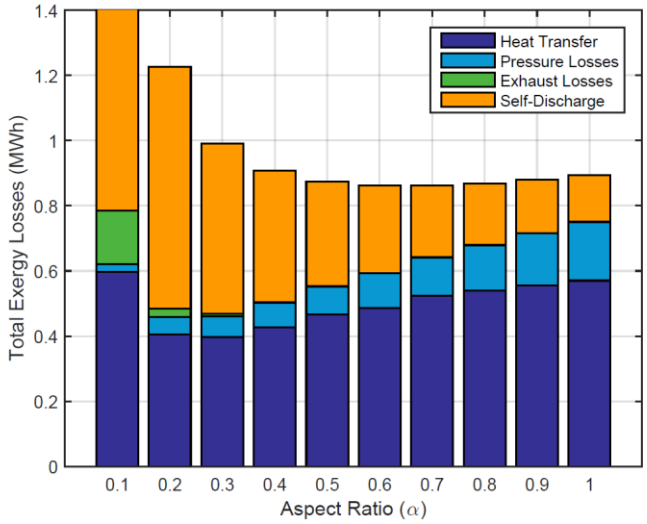

Figure 8. Contribution of the different mechanisms of exergy loss to the total losses of packed bed $\boldsymbol{A}$

It can also be seen in Figure 8 that the packed bed based on an α=0.7 achieves the lowest losses. This packed bed uses rocks with a diameter of 6.5 mm and incurs in roundtrip exergy losses of 0.865 MWh. This translates into an exergy efficiency of 97.4 %.

Figure 9a shows how the heat transfer exergy losses vary with different aspect ratios and rock sizes. These losses are directly proportional to the rock size and have an almost linear behaviour regardless of α. Heat transfer losses decrease with rock size because smaller particles provide a larger (total) contact area between the rocks and the stream of air. For reference, any one of the packed beds shown in the graph has 600 m^2 of heat transfer area per m^3 of rocks when 10 mm rocks are used. This increases to 6000 m^2/m^3 if the diameter of the rocks reduces to 1 mm. The available heat transfer area is a function of the total mass and size of the rocks and does not depend on the aspect ratio of the packed bed.

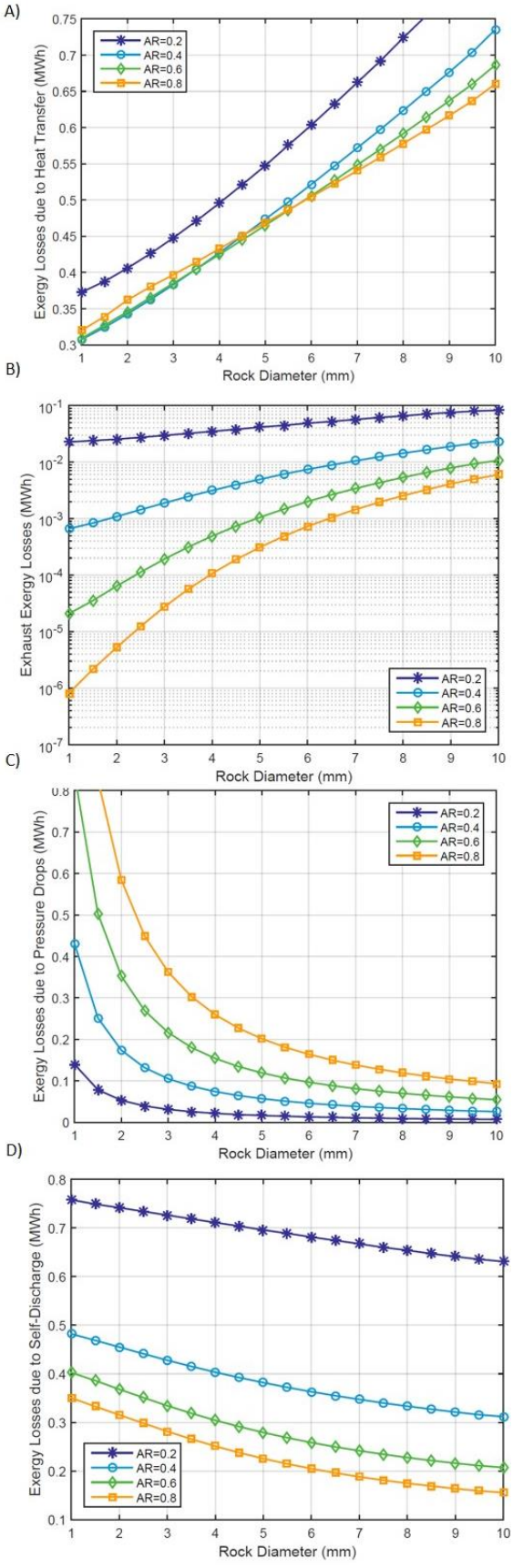

Figure 9. Behaviour of the different mechanisms of exergy loss with respect to changes in aspect ratio and rock size

Moreover, Figure 9a shows that heat transfer exergy losses are inversely proportional to α. The aspect ratio dictates the separation between the hot and cold ends of a packed bed. A greater height (large α) will lead to a sharper thermal front which in turn helps reducing heat transfer exergy losses.

If the thermal front was perfectly straight, the temperature of the cold end would remain constant at its nominal value throughout the charge of the store. On the other hand, a smoothed-out front causes the temperature of the cold end to rise. A higher-than-nominal temperature in the cold end at the end of the charging period will generate significant heat transfer losses during the following discharge period. Air at ambient temperature (290 K) will ingress the packed bed through its cold end and it will come in contact with rocks at a much higher temperature, which destroys exergy.

Furthermore, at the end of the discharge period, the temperature of the hot end of a packed bed based on a small α will be considerably below its nominal value due to the smoothed-out thermal gradient. This will generate further heat transfer losses during the following charging cycle as air enters the packed bed through the hot end at the nominal charging temperature (823.15 K) and comes into contact with rocks at a much lower temperature.

Figure 9b shows the behaviour of the exhaust losses with respect to the α and particle size used. Exhaust losses are directly proportional to the rock size. As aforementioned, the total available heat transfer area increases as the particle size reduces. Therefore when small rocks are used, a sharper thermal front is achieved which causes the air stream to exit the packed bed with a smaller amount of exergy left.

Figure 9b also shows that regardless of the rock size, exhaust losses reduce as α increases. A longer distance between the hot and cold ends of the packed bed helps to achieve a sharper thermal front, which as aforementioned, results in the air leaving the store at a lower temperature.

Figure 9c shows that the exergy losses due to pressure drops increase exponentially as the particle size reduces because the air stream faces a higher resistance to flow. It can also be seen that regardless of the rock size, larger values of α lead to much higher pressure losses. This increase in pressure drops is owed to two factors: A larger α means a greater bed height and a smaller cross sectional area, which causes faster velocities and consequently increased pressure losses (see Eqs. (7) and (9)).

Lastly, Figure 9d shows that self–discharge losses increase significantly as α reduces. Smaller aspect ratios entail a smaller separation between the hot and cold ends and a larger cross-section. Both dimensions facilitate the conduction of heat down the thermal front. In packed beds based on very small values of α, self-discharge losses are the major source of exergy loss.

Figure 10 shows the evolution of the thermal front of the optimum packed designed for $\boldsymbol{A}$. The figure compares the results obtained when the geometry is discretized in 200 slices (elements) against those obtained when it is divided into 800 slices. It was found in previous work [38,39] that accurate results (for packed beds of similar physical sizes) could be obtained using 200 slices in the mathematical model. It can be seen in the figure that the differences between the two sets of results (200 vs 800 slices) are almost negligible despite having quadruplicated the amount of elements in the geometry. It can therefore be concluded that discretizing the geometry into 200 elements allows capturing the shape of the thermal front, which is the basis for all exergy loss calculations. The rest of the optimization work in this study is carried out using 200 slices for the spatial discretization of the packed beds.

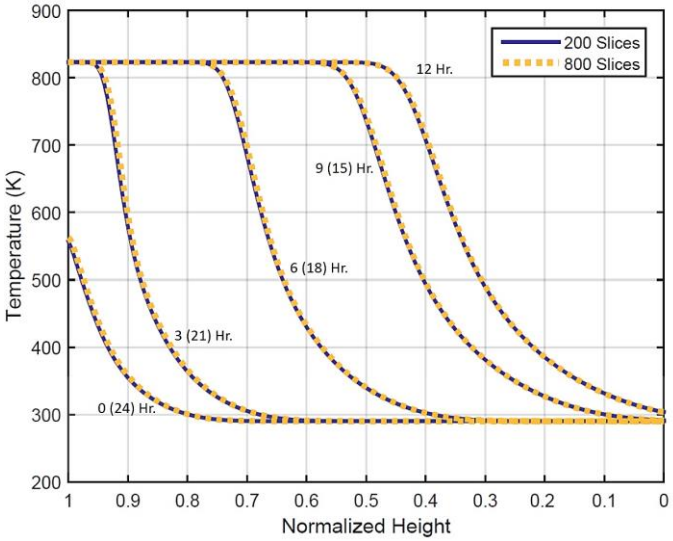

Figure 10. Evolution of the thermal front of packed bed optimized for work-cycle $\boldsymbol{A}$ (α= 7, 6.5mm rocks)

4.2 Results obtained for the low-frequency packed bed (B)

This section is concerned with the design and optimization of the packed beds for the different low-frequency profiles ($\boldsymbol{B}$) corresponding to the different work-cycle splits. The profiles have been shown in Figure 5.

The results of the optimization process for each value of K_B are shown in Figure 11. The designs presented for each value of α consider the optimum size of rocks for that specific geometry. The exergy losses have been normalized with respect to the exergy input to allow a direct comparison between the different capacity ratios (K_B). It should be remembered that a larger K_B has a larger exergy input.

Figure 11 reveals that the exhaust exergy losses are a major contributor to the total exergy losses of the packed beds for work-cycles with small capacity ratios ($K_B \leq 0.6$). In this range, exhaust losses account for 34-44% (depending on α) of the total exergy losses seen by the different packed beds.

Exhaust exergy losses decrease as the capacity ratio increases until the point where they become almost negligible (K_B=0.99). For any one value of K_B , exhaust losses reduce as α increases because a greater separation between the hot and cold ends of the packed bed helps the air to come out of the store at a lower temperature. Similarly, for any given value of α, exhaust losses decrease as the capacity ratio increases. A larger K_B implies a larger storage capacity which translates into a bigger packed bed with a larger separation between its ends.

Figure 11 also shows that self-discharge exergy losses have a similar behaviour to the exhaust losses. For any value of K_B, self-discharge losses reduce as α increases. These losses consist mostly on heat being conducted down the thermal gradient; thus a taller packed bed will experience reduced (or slowed-down) self-discharge losses. For this same reason, self-discharge losses decrease as the capacity ratio increases.

In some cases, self-discharge exergy losses account for a big share of the total losses of the packed bed. For instance in designs based on a small aspect ratio ($0.2 \leq \alpha \leq 0.5$), self-discharge losses account for between 30 and 62% of the total exergy losses. On the other hand, in designs based on a larger aspect ratio ($0.8 \leq \alpha \leq 1.0$), self-discharge losses represent between 12 and 28% of the total losses of the packed bed.

Exergy losses due to pressure drops are generally speaking, the least troublesome form of exergy loss. Figure 11 shows that for any capacity ratio, these losses increase as α increases. This is owed to the fact that a larger aspect ratio entails that the same mass of air is flowing through a smaller cross-section and has to travel a longer distance. For any given K_B, the cross-sections of packed beds with an α=0.6 and an α=1.0 are 52% and 66% smaller than the cross-section of a design based on an α=0.2. At the same time, the height of those same two packed beds are two and three times larger than the height of the packed bed based on an α=0.2.

It can also be seen in Figure 11 that the exergy losses due to pressure drops have a general tendency to increase with increasing values of K_B. The reason behind this is not related to the simple fact that a larger capacity ratio entails a higher peak (and RMS) power, because the physical dimensions of the packed bed enlarge as well. In this particular case, the *RPtS* ratio of the different $\boldsymbol{B}$ work-profiles increase as the capacity ratio (K_B) increases. Although this increase is not dramatic, it is enough to worsen the pressure-related exergy losses. The increase in the *RPtS* ratio is intrinsically related to the shape of the work-cycle $\boldsymbol{A}$ and the way the sign-preserving filter works. It is very well possible that a different behaviour would be observed if a different signal $\boldsymbol{A}$ was used.

The optimum rock size becomes smaller as the capacity ratio increases because a greater (dis)charging power requires a larger heat transfer area. For instance, the optimum packed bed for a $K_B = 0.5$ has an α=0.5 and uses 6 mm rocks. This gives the packed bed 8846 m^2 of total heat transfer area per kWh of exergy input. In contrast, the optimum packed bed for a $K_B = 0.8$ has an α=0.7 but uses rocks with a diameter of 4 mm, which translates into 13695 m^2 per kWh of exergy input. The reduction in particle size is a consequence of the optimizer's efforts to achieve good heat transfer capabilities. However, pressure drops are aggravated by the use of smaller sized rocks, as Eq. (9) indicates.

Heat transfer exergy losses exhibit a different behaviour to the other three mechanisms of exergy loss already discussed. This form of exergy loss has optimum points which are a consequence of the optimizer's attempts to minimize the other sources of exergy loss. Figure 11 shows that at small capacity ratios, packed beds based on large aspect ratios experience substantial heat transfer losses due to the fact that the rock size was increased as a measure to counteract pressure drops.

Two general trends for the heat transfer exergy losses can be identified. 1) These losses reduce as α becomes smaller. The larger cross-section of the container helps to control pressure losses; therefore the optimizer can use smaller rocks which promote a better heat transfer. 2) For a given value of α, a small capacity ratio maximizes the heat transfer exergy losses. Heat transfer exergy losses start decreasing as K_B increases, until reaching a minimum in the region between 0.6≤K_B≤0.8.

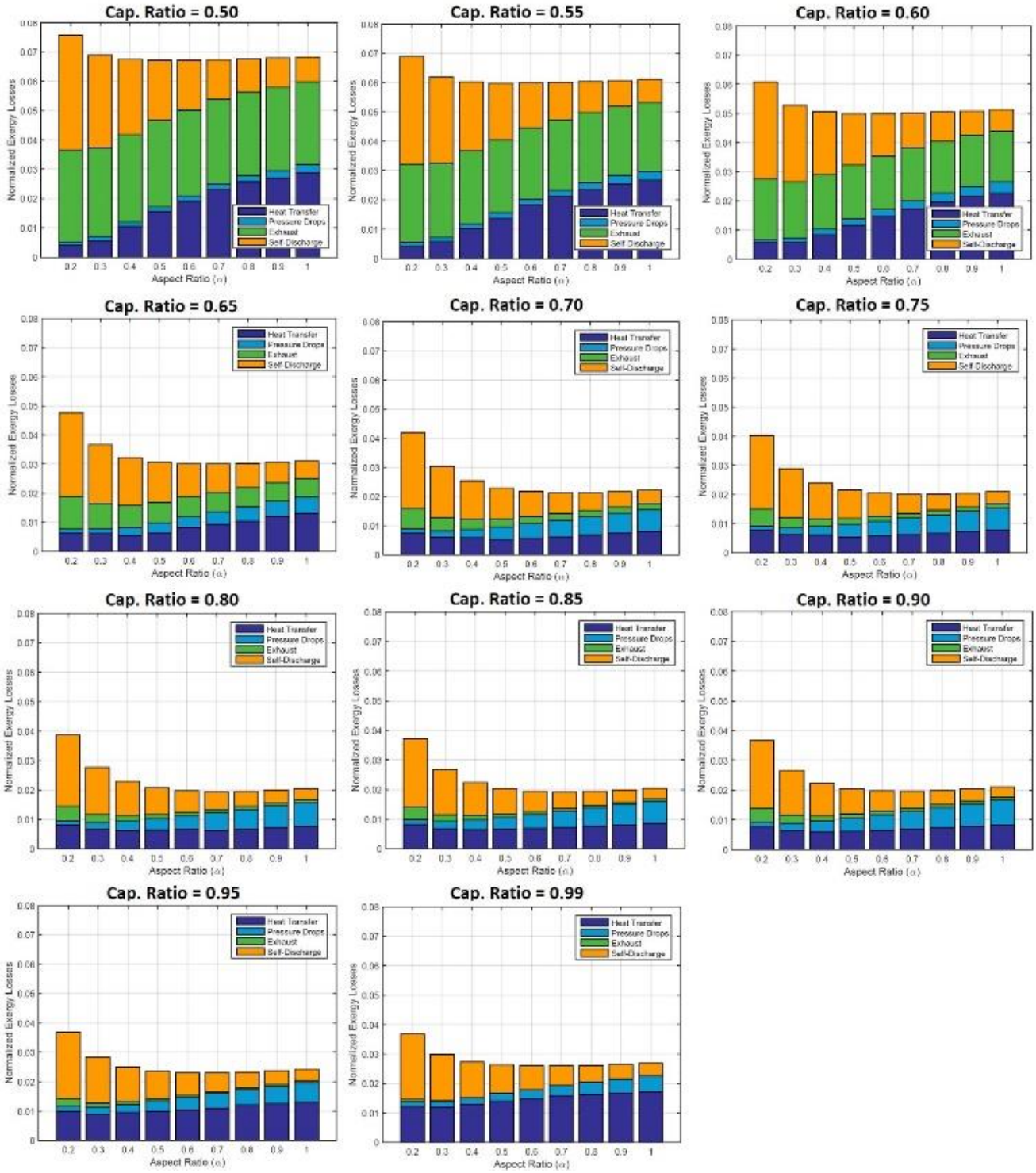

Figure 11. Normalized exergy losses of designs for packed bed $\boldsymbol{B}$ considering different values of α and K_B

Figure 12 shows a set of surface plots that have been generated from the information presented in Figure 11. These plots provide a different view of the effect that the aspect ratio (α) and the capacity ratio (K_B) have on the behaviour of the different forms of exergy loss.

Figure 13 shows the total exergy losses of the optimum designs (combination of α + rock size) for each one of the different capacity ratios. It should be noted that the values shown in Figure 13 are total net exergy losses instead of being normalized with respect to the exergy input, as it was the case of previous figures.

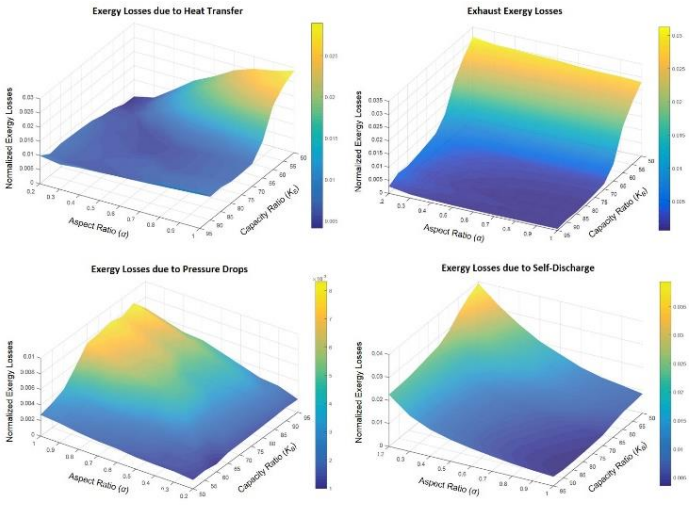

Figure 12. Behaviour of the mechanisms of exergy loss (normalized) as the values of α and K_B are varied.

It can be seen from Figure 13 that as K_B approaches a value of one, the exergy losses of packed bed $\boldsymbol{B}$ approach the reference value (0.865 MWh). At this point the two work-cycles ($\boldsymbol{B}$ and $\boldsymbol{A}$) are almost identical, therefore the packed beds are very similar to each other. Designs based on a $K_B \leq 0.63$ are automatically discarded because their roundtrip exergy losses exceed the target value without even considering the losses of packed bed $\boldsymbol{C}$.

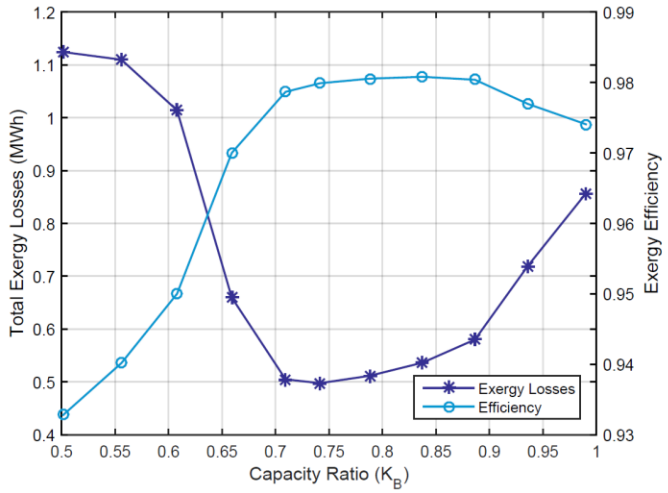

Figure 13. Total exergy losses of the best packed bed $\boldsymbol{B}$ (α+ rock size) for each one of the different capacity ratios

Figure 13 reveals a region of "low exergy losses" between capacity ratios of 0.68 and 0.85. Within this region, the packed bed for a capacity ratio of 0.75 achieved the lowest roundtrip exergy losses (0.4975 MWh). This packed bed considers an α of 0.7 and uses rocks with a diameter of 4mm. It is noteworthy that despite having the lowest losses, the packed bed for K_B=0.75 does not have the highest efficiency.

It is equally important to emphasize that although packed bed $\boldsymbol{B}$ obtained the lowest exergy losses with a $K_B = 0.75$, this capacity ratio cannot be considered yet as the optimum split of the work-cycle because the exergy losses of packed bed $\boldsymbol{C}$ still need to be accounted for. It could be the case that the sum of the losses of packed beds $\boldsymbol{B}$ and $\boldsymbol{C}$ for a different capacity ratio is lower than the combined losses seen with a $K_B = 0.75$.

4.3 Results obtained for the high-frequency packed bed (C)

This section is concerned with the design/optimization of the packed beds for the different high-frequency profiles ($\boldsymbol{C}$) corresponding to the different work-cycle splits. These profiles have been previously shown in Figure 5.

Figure 14 shows the optimization process for each one of the work-cycles considered. In the figure, several packed bed designs are presented for each capacity ratio. Each of the designs shown has a different α and considers the optimum size of rocks for that specific configuration. The exergy losses are normalized with respect to the exergy input of the work-cycle to allow a comparison between different work-cycles. It is important to remember that the capacity ratio is expressed in terms of packed bed $\boldsymbol{B}$; for example, a K_B of 0.6 means that packed bed $\boldsymbol{C}$ is providing 40% of the total energy storage capacity.

Figure 14 reveals that self-discharge exergy losses are in all cases a major contributor to the total exergy losses of the packed beds. For any given capacity ratio, self-discharge losses increase as the aspect ratio reduces because a smaller α entails a shorter distance between the hot and cold ends of the packed bed. In designs based on small values of α (0.2 to 0.5), self-discharge losses account for between 50-70% of the total exergy losses of the packed beds.

It is also possible to see that for any given value of α, exergy losses due to self-discharge increase as the capacity ratio of the work-cycle increases. A larger K_B translates into a smaller sized packed bed $\boldsymbol{C}$; as aforementioned, reducing the height of the packed bed intensifies self-discharge losses.

Exhaust losses exhibit a similar behaviour to self-discharge losses, although for the case of packed bed $\boldsymbol{C}$ they are not as critical. For any K_B, exhaust losses increase with α. A taller container helps to maintain a sharper thermal front, which in turn results in the air leaving the store with less exergy left.

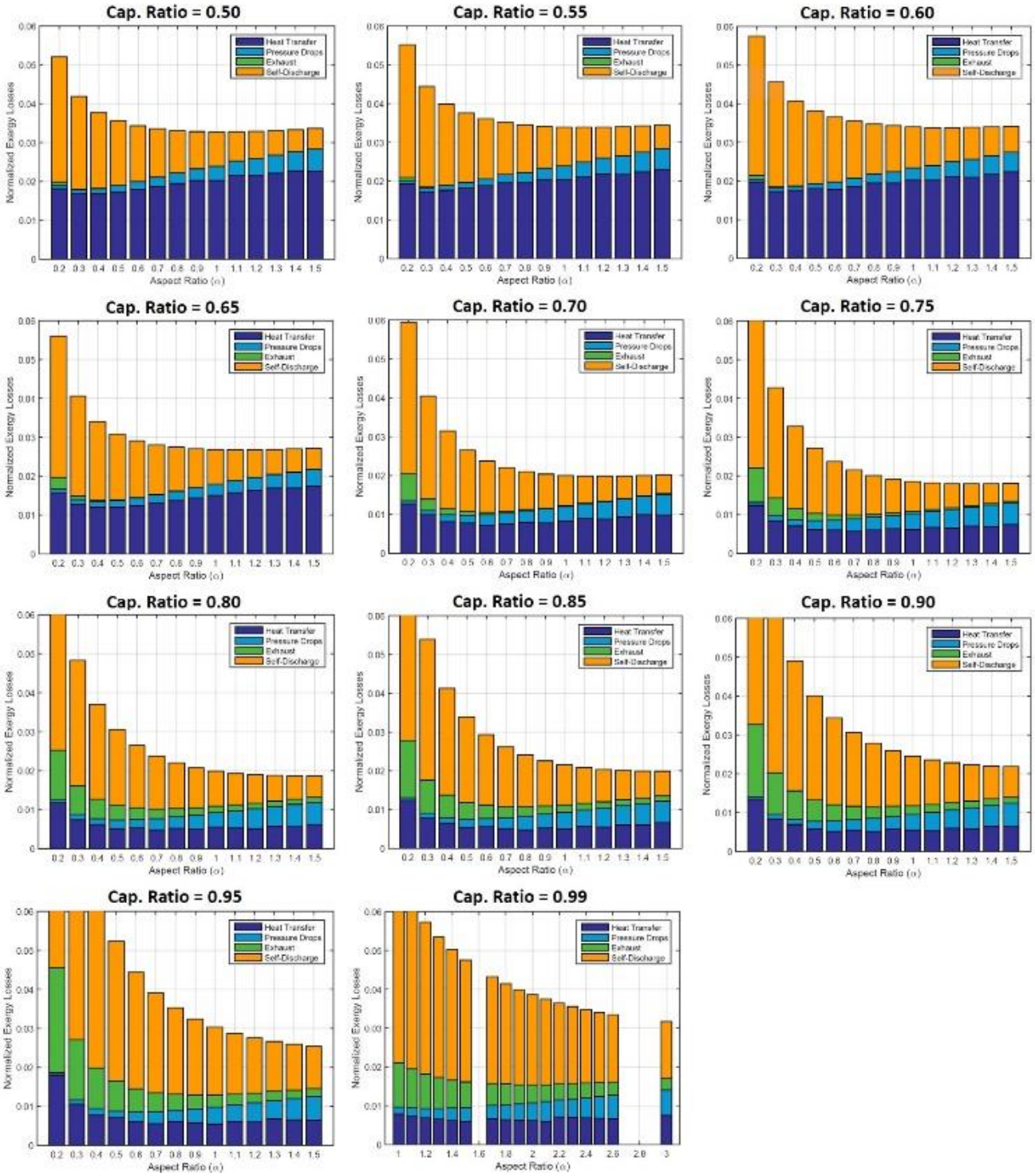

Figure 14. Normalized exergy losses of different designs of packed beds for different work-cycles $\boldsymbol{C}$

Figure 14 also shows that for any given value of α, exhaust losses increase with an increasing capacity ratio because the volume and height of the packed bed reduce as the value of K_B rises. Exhaust losses are almost negligible in packed beds designed for small capacity ratios ($0.5 \leq K_B \leq 0.6$), accounting for less than 1.5% of the total exergy losses. On the other hand, in packed beds designed for large capacity ratios ($K_B \geq 0.85$), exhaust losses represent (depending on α) between 7-20% of the total exergy losses.

Similar to what was seen in the optimization of packed bed $\boldsymbol{B}$, the exergy losses caused by pressure drops have a tendency to increase with increasing values of α (for any given K_B) because the container's cross-section reduces, its height

enlarges and the mass flow of air stays the same. For any capacity ratio (K_B), the optimum rock size for packed bed $\boldsymbol{C}$ increases with aspect ratio in order to control pressure drops. However the reduced cross-section has a stronger effect on the pressure drops, therefore these losses increase considerably with increasing values of α. It can be seen in Figure 14 that for any value of K_B, pressure drops represent between 15-30% of the total exergy losses of designs based on large aspect ratios ($1.3 \leq \alpha \leq 1.5$) while in designs with a small aspect ratio ($0.2 \leq \alpha \leq 0.4$) they account for 5% or less.

It can also be seen in Figure 14 that the exergy losses due to pressure drops have a tendency to increase as the capacity ratio increases, which in the case of packed bed $\boldsymbol{C}$ means that the size of the store is reducing. This tendency is not very pronounced. As the capacity ratio (K_B) increases, the work-cycles $\boldsymbol{C}$ become purer high-frequency signals (see Fig.5). Accordingly, the optimization algorithm will employ smaller sized rocks to enhance the heat transfer capabilities of the packed bed. A smaller particle size entails increased pressure drops. Furthermore, very high capacity ratios translate into very small packed beds $\boldsymbol{C}$. These packed beds have a high *RPtS* ratio (see Table 3) which also contributes to having increased pressure drops since a larger mass flow of air is pumped through a narrower container.

The behaviour of the heat transfer exergy losses is noticeably different to that of the other forms of exergy loss. Instead of increasing or decreasing continuously with K_B and/or α, heat transfer losses have an optimum region. For a given capacity ratio, packed beds with a large aspect ratio experience elevated exergy losses due to heat transfer. The losses reduce as α decreases but after a region between $0.3 \leq \alpha \leq 0.5$ they start increasing again. In designs based on large aspect ratios, rocks with a large diameter (between 3-8 mm) are used to alleviate pressure drops; however the diminished overall surface area affects the heat transfer properties of the packed bed.

Exergy losses due to pressure drops stop being critical in designs based on small aspect ratios due to the larger cross-section of the container; therefore rocks with a smaller diameter (<2mm) can be employed to improve heat transfer. However, the reduced height (consequence of a small α) affects the sharpness of the thermal front. A smeared thermal front will produce heat transfer losses throughout the geometry of the packed bed in addition to considerable exhaust losses during the charging period because the cold end of the store departs from its nominal temperature. This rise in the temperature of the cold end will also produce substantial heat transfer losses during the subsequent discharging period.

For work-cycles with a K_B between 0.5 and 0.65, heat transfer losses account for between 50 and 68% of the total exergy losses seen by packed beds designed with values of α ranging from 0.8 to 1.5. In contrast, for work-cycles with a K_B≥0.8, heat transfer losses only represent between 17 and 30% of the total exergy losses of packed beds based on the same range of aspect ratios.

For any one value of α, the contribution (%) of the heat transfer losses to the total exergy losses reduces as the capacity ratio of the work-cycle increases (K_B). If the work-cycle split has a larger capacity ratio, the resultant signal $\boldsymbol{C}$ will have a smaller amount of low-frequency content (see Fig.5); in other words, the signal $\boldsymbol{C}$ will be more purely a high frequency profile. Consequently, as K_B increases for a constant aspect ratio, the optimizer will use smaller rocks to increase the available heat transfer area and enable the packed bed to deal more effectively with the fast-frequencies of the work-cycle. For example, a packed bed with a K_B=0.5 and an α=0.8 uses rocks with a diameter of 5.5mm, which yields to a total of 10295 m^2 per kWh of exergy input. On the other hand, a packed bed for a K_B =0.9 and the same aspect ratio, utilizes 2.5mm rocks. This increases the available heat transfer area to 21893 m^2 per kWh of exergy input.

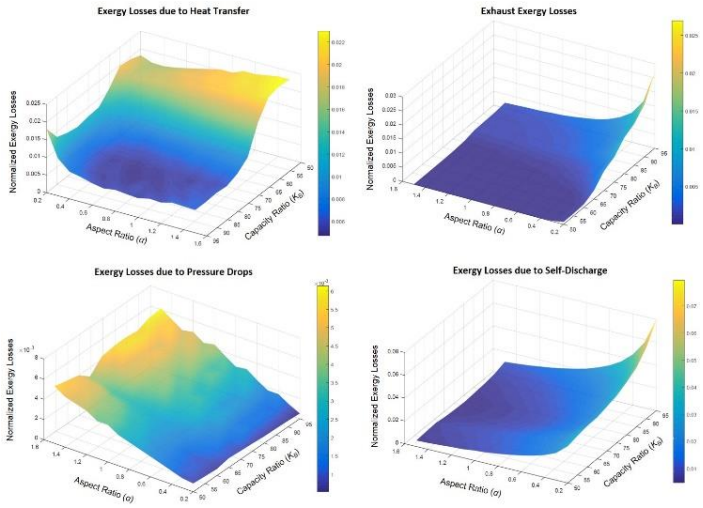

Figure 15. Behaviour of different forms of exergy loss (normalized) with respect to changes in the aspect ratio (α) and capacity ratio (K_B)

A set of surface plots that summarize the information discussed above is presented in Figure 15. These plots provide

a clear overview of the behaviour of the different types of exergy loss with respect to changes in two design parameters: the capacity ratio of the work-cycle (K_B) and the aspect ratio (α) of the packed bed.

Figure 16 shows the total exergy losses of the optimum designs (combination α and rock size) for each one of the different capacity ratios explored. It should be noted that the losses displayed in the figure are net total losses instead of normalized values with respect to the exergy input.

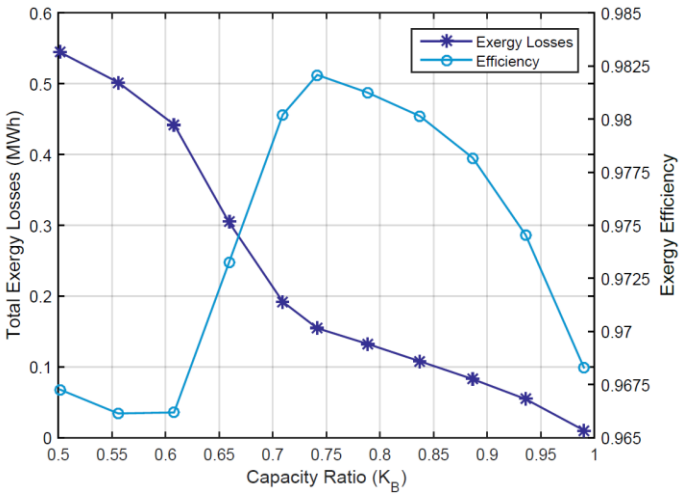

Figure 16. Total exergy losses of the best design of packed bed $\boldsymbol{C}$ (α + rock size) for each one of the different capacity ratios explored.

The behaviour of the net exergy losses shown in Figure 16 differs greatly from that observed during the optimization of packed bed $\boldsymbol{B}$ (section 4.2). The net exergy losses are almost zero at a capacity ratio of 0.99; however this observation is to some extent trivial because at a K_B=0.99 there is very little exergy being stored in the packed bed, hence losses are small. Net exergy losses are at a maximum (within the range explored) for a K_B=0.5 because at that point the maximum amount of exergy is being passed through the store.

The most efficient design is found for a capacity ratio of 0.75; however, it cannot be considered yet as the optimum work-cycle split. The global optimum is the work-cycle split (indicated by K_B) that minimizes the sum of the losses of packed beds $\boldsymbol{B}$ and $\boldsymbol{C}$.

4.4 Overall results achieved by the load-based optimization

This section presents the overall results of the load–based optimization carried out. Figure 17 shows the combined exergy losses of packed beds $\boldsymbol{B}$ and $\boldsymbol{C}$ for the different work-cycles that were explored. The individual contributions of the two packed beds, which were previously presented in figures 13 and 16, are also shown in the figure. The roundtrip exergy losses attained by the packed bed optimized for the working cycle $\boldsymbol{A}$ are displayed by a red horizontal line at 0.865 MWh. These losses are the target for the load-based optimization.

It can be seen at a first glance that for duty-cycle splits with a capacity ratio (K_B) of 0.65 or lower, the performance of the combined system ($\boldsymbol{B}$+$\boldsymbol{C}$) is worse than the reference case ($\boldsymbol{A}$); in some cases the total exergy losses are almost doubled. These work-cycles are automatically discarded. Work-cycle splits done with a capacity ratio in the region 0.7≤K_B≤0.95 achieve losses below the target value. The best split is obtained with a nominal capacity ratio of 0.85.

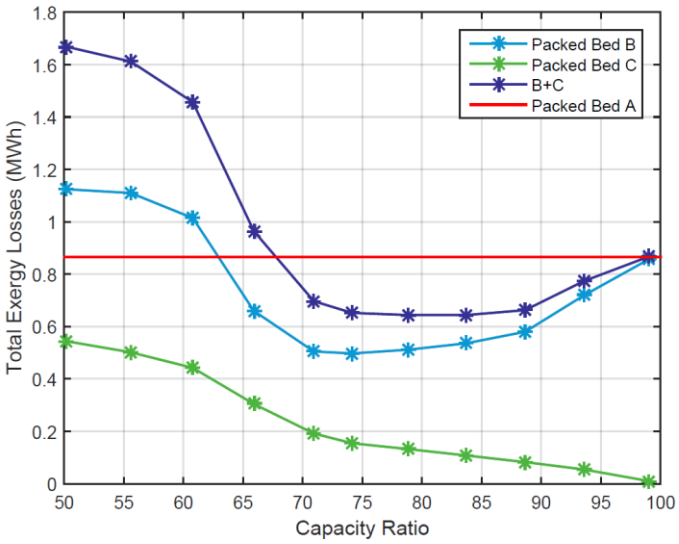

Figure 17. Exergy losses of packed beds $\boldsymbol{B}$ and $\boldsymbol{C}$ optimized for the different capacity ratios explored.

The packed bed $\boldsymbol{B}$ for this particular load split ($K_B = 0.85$) is considers an aspect ratio of 0.7 and uses rocks with a diameter of 4.5 mm. This packed bed has 0.5362 MWh of exergy losses throughout a working cycle, which translates into a roundtrip exergy efficiency of 98.08 %.

On the other hand, the packed bed $\boldsymbol{C}$ for this particular load-split is designed with an aspect ratio of 1.5 and uses rocks with a diameter of 4.5mm. With this design, the packed bed achieves 0.1078 MWh of exergy losses at the end of a full working cycle, which represents a roundtrip exergy efficiency of 98.02%.

The combined exergy losses of packed beds $\boldsymbol{B}$ and $\boldsymbol{C}$ for a capacity ratio of 0.85 are 0.644 MWh. This represents a reduction of 25.5 % with respect to the losses of packed bed $\boldsymbol{A}$

(i.e. 'target' value). Table 4 summarizes the most relevant design and performance parameters of the optimum packed beds for the two work-profiles $\boldsymbol{B}$ and $\boldsymbol{C}$ for a capacity ratio of K_B=0.85. Figure 18 shows for comparison, the temperature gradients of the three packed beds at different times during their operation.

Table 4. Parameters of packed beds $\boldsymbol{B}$ and $\boldsymbol{C}$ designed for the optimum work-cycle split (K_B=0.85)

	Parameters	Packed Bed A	Packed Bed B	Packed Bed C
Geometrical	Mass overrating factor	1.5	1.5	1.5
	Total mass of rock (kg)	807019	675740	131286
	Volume of rock (m^3)	304.54	254.99	49.54
	Void fraction	0.395	0.395	0.395
	Particle size (mm)	6.5	4.5	4.5
	Heat transfer area per vol. or rock (m^2/m^3)	923.1	1333.3	1333.3
	Aspect ratio (α)	0.7	0.7	1.5
	Container diameter (m)	9.71	9.15	4.11
	Container height (m)	6.79	6.41	6.17
	Container surface area (m^2)	355.62	315.92	106.26
Operational	Max. Air flow rate (kg/s)	17.97	16.16	3.65
	Max. Inlet pressure (Bar)	1.022	1.026	1.032
	Max. Air velocity (m/s)	0.566	0.573	0.634
	Max. Heat transfer coefficient (W/m^2K)	79.96	80.48	85.74
	Total exergy input (MWh)	33.48	28.02	5.52
	Temp. Hot end @ 24 hr (K)	558.38	723.61	810.69
	Temp. Cold end @ 12 hr (K)	304.08	342.36	423.55
Performance	Ex. Losses due to heat transfer (kWh)	525.7	201.27	35.94
	Ex. Losses due to pressure drops (kWh)	117.7	154.73	29.95
	Exhaust exergy losses(kWh)	1.6	22.17	7.72
	Ex. Losses due to self-discharge(kWh)	220	158.1	34.17
	Roundtrip exergy efficiency (%)	97.4	98.08	98.02

It should be mentioned that the signal-split that obtained the lowest exergy losses (K_B=0.85) may not be the true optimum. Remembering the discussion presented in section 3.1, the two-dimensional space of signal splits was reduced to only one dimension by means of the "capacity ratio". Eleven different signal-splits evenly distributed in the range 0.5≤K_B≤0.99 were selected and used for the simulations.

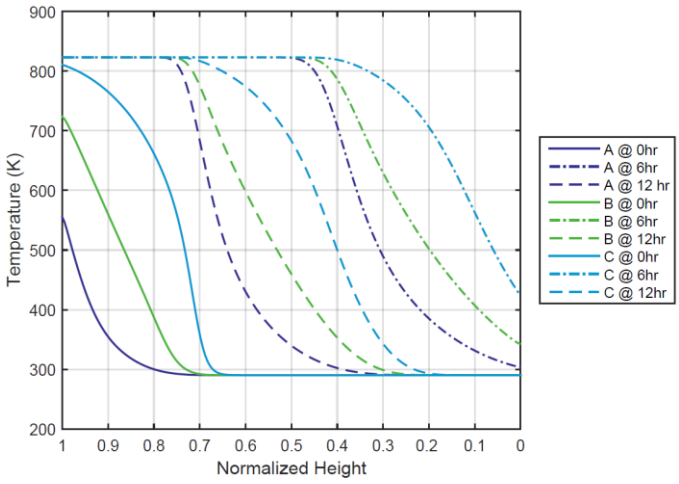

Figure 18. Thermal fronts of packed beds $\boldsymbol{B}$ **(green)** and $\boldsymbol{C}$ (cyan) for K_B=0.85 at different times during operation

If the two-dimensional search space was fully explored, it would be found that the signal-split that produces the lowest exergy losses is created with a different combination of w_{max} and n_{runs} (filter's parameters) and that it has a different capacity ratio. However, an exhaustive exploration of the space would be very computationally expensive and almost impracticable. It is clear from Figure 17 that the optimum found in the simplified search space lies very close to the real optimal solution given the flatness of the curve in the region 0.7≤K_B≤0.95.

The results obtained from the load-based optimization are very promising. As table 4 shows, the total storage mass does not increase when packed bed $\boldsymbol{A}$ is separated into two independent packed beds $\boldsymbol{B}$ and $\boldsymbol{C}$. The foregoing means that it is possible to design, at a marginal additional cost, a two-packed bed system ($\boldsymbol{B}$+$\boldsymbol{C}$) that performs the same function as the single packed bed $\boldsymbol{A}$ but incurs in 25.5% less losses in doing so.

The "load-based optimization" approach proposed could be used for example, to optimize a packed bed intended for working as a standalone industrial waste heat recovery unit [53] or to optimize the thermal store of a compressed air energy storage (CAES) system [54]. In this case the only modification that the CAES system will suffer is having two packed beds instead of one. All the components of the system located before the thermal store (compression train, heat exchangers) and after the thermal store (compressed air reservoir, expansion train) will remain unmodified.

The implementation of the two-packed bed thermal store entails an additional—albeit small—cost. A greater amount of structural steel will be required for the two containers and there will be a larger surface area to insulate. In addition to that two simple "Y-type" manifolds will be needed, one for charging the packed beds and one for discharging them. Each manifold is equipped with a pair of valves, which are the devices in charge of physically splitting the signal $\boldsymbol{A}$.

During the charging mode, the compression train will operate under the work-profile $\boldsymbol{A}$, which is the duty for which the system is required. The high-pressure air coming from the compression train is circulated through a heat exchanger where it transfers its heat to a secondary stream of ambient pressure air, same as in a normal CAES system. A controller unit operates the valves in the manifold to split the flow of low-pressure air into two separate streams $\boldsymbol{B}$ and $\boldsymbol{C}$ for the two independent packed beds. It is worth noting that the cost of the controller is negligible in comparison to the rest of the system. The controller has predetermined values of how much air mass (power) should go to each one of the packed beds at any given time during the work-cycle and controls the position of the valves to split the incoming flow accordingly.

The load-based optimization described in this paper presupposes knowing in advance the load profile $\mathbf{A}$ in order to determine the optimum split and design the packed beds $\mathbf{B}$ and $\mathbf{C}$ that will service the two frequency components. For this reason, this optimization technique is not very well suited for designing energy stores intended for working alongside variable renewable generation. The load-based optimization is particularly helpful for designing systems that will operate under a known duty-cycle in applications such as energy arbitrage or waste heat recovery.

An energy storage system can operate under a different work-cycle to the one it was optimized for; however a sub-optimal performance will be observed. This 'drawback' is not exclusive of the load-based optimization approach presented herein; the design of thermo-mechanical energy storage systems (including packed beds) always involves some form of optimization that considers a representative signal. The systems have the ability to deviate from their ideal operation at the expense of some efficiency.

If it is desired to use the load-based optimization approach in an application with a variable load $\boldsymbol{A}$, it behoves the designer to estimate how much the work-cycle will vary over time and evaluate if the performance attained by the packed beds $\boldsymbol{B}$ and $\boldsymbol{C}$ when operating under the future conditions is still acceptable and/or better than the performance achievable by a single packed bed.

If a two-bed thermal store was already built and for some unexpected reason the load $\boldsymbol{A}$ was modified, a new load-based optimization could be carried out to determine the split of the new profile $\boldsymbol{A}$ that makes the most efficient use of the two existing packed beds $\boldsymbol{B}$ and $\boldsymbol{C}$.

It is important to highlight that the study presented in this paper is only an example to demonstrate that the performance of a packed bed can be improved using the "load-based optimization" approach. In this case-study a 25.5% reduction in the overall exergy losses was achieved. However, the applicability and success of this optimization technique depend heavily on the shape, type and amount of high-frequencies of the reference signal. There may be cases in which using multiple (2 or more) parallel packed beds for servicing different frequency components of the duty-cycle will not yield an improvement in the overall performance of the thermal store. Conversely, there may be cases where the reduction in the exergy losses achieved is much greater than 25%.

5. Concluding Remarks

In this paper, a load-based approach for optimizing a packed bed has been presented. The optimization method proposed consists in splitting the work-cycle into two profiles, a mostly low-frequency signal ($\boldsymbol{B}$) and a mostly high frequency signal ($\boldsymbol{C}$). Each one of the frequency components is handled by a separate packed which has been expressly designed and optimized for it.

A 'sign-preserving filter' that allows separating a work-cycle into two signals that have the same sign at all times was developed and used for this work. The case-study presented in the paper uses a sinusoidal profile with some added noise as the working cycle ($\boldsymbol{A}$) for a packed bed. The profile is a 24 hour-long cycle that comprises a 12-hr charging period and a 12-hr discharge. The peak power of the cycle is 10 MW and the energy throughput is 76.3 MWh or 33.3 MWh of exergy if a charging temperature of 550°C is considered, which is typical of a CAES system.

A packed bed was designed and optimized for the work-cycle $\boldsymbol{A}$ using a mathematical model that allows varying the aspect ratio and the rock size. This packed bed is the 'reference case'

for the study. It was found that the best possible design for this particular cycle has an aspect ratio of 0.7 and uses 807.02 tons of rocks with a diameter of 6.5 mm. The roundtrip exergy losses of this packed bed are 0.865 MWh, which translates into an exergy efficiency of 97.4 %.

Several different work-cycle splits were analyzed. Many of them attained combined losses ($\boldsymbol{B}+\boldsymbol{C}$) below those of the reference case. The optimum work-cycle split has a capacity ratio (K_B) of 0.85, which means that the low-frequency packed bed $\boldsymbol{B}$ provides 85% of the total energy storage capacity. The optimum packed bed for the low-frequency signal ($\boldsymbol{B}$) has an aspect ratio of 0.7, uses 675.74 tons of rock and incurs in 0.536 MWh of exergy losses throughout the work-cycle. On the other hand, the optimum packed bed for the high frequency signal ($\boldsymbol{C}$) is based on an aspect ratio of 1.5, uses 131.29 tons of rock and generates 0.1078 MWh of exergy loss per work-cycle. The combined losses of the two packed beds are 0.644 MWh, which translates in an overall exergy efficiency of 98.07%. In short, the two-packed bed system ($\boldsymbol{B}+\boldsymbol{C}$) performs the same function as the single packed bed $\boldsymbol{A}$ but has 25.5% less exergy losses.

The case study presented is just an example that demonstrates that the performance of a packed bed can be improved by splitting its load into frequency components. The approach can be used in other optimization problems where the design of a component would benefit from an input signal with a narrower range of frequencies.

It is also important to highlight that in the particular case-study presented in this paper, a 25.5% reduction in the overall exergy losses was achieved. However, the applicability and results of the load-based optimization depend heavily on the shape, type and amount of high-frequency content of the reference signal. There may be cases in which using multiple parallel packed beds for servicing different frequency components of the duty-cycle will not improve the overall performance of the thermal store and there may be cases in which the performance improvement is much more pronounced.

Acknowledgements

This research work has been funded by the United Kingdom's Engineering and Physical Sciences Research Council (EPSRC) through the following projects: "Next Generation Grid Scale Thermal Energy Storage Technologies" (NexGen-TEST: EP/L014211/1) and "Multi-scale Analysis for Facilities for Energy Storage" (Manifest: EP/N032888/1).

References

[1] A.Castillo, D.F.Gayme. Grid-scale energy storage applications in renewable energy integration: A survey. Energy Conversion and Management 2014; 87:885-894.

[2] M.Aneke, M.Wang. Energy storage technologies and real life applications – A state of the art review. Applied Energy 2016; 179: 350–377

[3] K. Bassett, R.Carriveau, D.S.K.Ting. Energy arbitrage and market opportunities for energy storage facilities in Ontario. Journal of Energy Storage 2018; 20:478-484.

[4] B. Lin, W. Wu, M. Bai, C. Xie, J. Radcliffe. Liquid air energy storage: Price arbitrage operations and sizing optimization in the GB real-time electricity market. Energy Economics 2019; 78: 647-655.

[5] L. Miró, J. Gasia, L.F. Cabeza. Thermal energy storage (TES) for industrial waste heat (IWH) recovery: A review. Applied Energy 2016; 179:284-301

[6] W.D. Steinmann. Thermo-mechanical concepts for bulk energy storage. Renewable and Sustainable Energy Reviews 2017; 75: 205-219.

[7] L. Geissbühler, V. Becattini, G. Zanganeh, S. Zavattoni, M. Barbato, A. Haselbacher, A. Steinfeld. Pilot-scale demonstration of advanced adiabatic compressed air energy storage, Part 1: Plant description and tests with sensible thermal-energy storage. Journal of Energy Storage 2018; 17:129-139

[8] A. Sciacovelli, Y. Li, H. Chen, Y. Wu, J. Wang, S. Garvey, Y. Ding. Dynamic simulation of Adiabatic Compressed Air Energy Storage (A-CAES) plant with integrated thermal storage – Link between components performance and plant performance. Applied Energy 2017; 185:16-28.

[9] E. Barbour, D. Mignard, Y. Ding, Y. Li. Adiabatic compressed air energy storage with packed bed thermal energy storage. Applied Energy 2015; 155: 804–815.

[10] H. Peng, X. Shan, Y. Yang, X. Ling. A study on performance of a liquid air energy storage system with packed bed units. Applied Energy 2018; 211: 126-135.

[11] A. Sciacovelli, A. Vecchi, Y. Ding. Liquid air energy storage (LAES) with packed bed cold thermal storage – From component to system level performance through dynamic modelling. Applied Energy 2017; 190: 84-98.

[12] R. Morgan, S. Nelmes, E. Gibson, G. Brett. Liquid air energy storage – Analysis and first results from a pilot scale demonstration plant. Applied Energy 2015; 137: 845-853.

[13] P.Farres-Antunez, H.Xue, A.J. White. Thermodynamic analysis and optimisation of a combined liquid air and pumped thermal energy storage cycle. Journal of Energy Storage 2018; 18: 90-102.

[14] J.D. McTigue, A.J. White, C.N. Markides. Parametric studies and optimisation of pumped thermal electricity storage. Applied Energy 2015; 137: 800–811

[15] A. White, G. Parks, C.N. Markides. Thermodynamic analysis of pumped thermal electricity storage. Applied Thermal Engineering 2013; 53:291-298.

[16] B. Yang, F. Bai, Y. Wang, Z. Wang. Study on standby process of an air-based solid packed bed for flexible high temperature heat storage: Experimental results and modelling. Applied Energy 2019; 238: 135–146.

[17] T.R.G. Davenne, S.D. Garvey, B. Cardenas, J.P. Rouse. Stability of packed bed thermoclines. Journal of Energy Storage 2018; 19: 192–200.

[18] T. Esence, A. Bruch, J.F. Fourmigue, B. Stutz. A versatile one-dimensional numerical model for packed-bed heat storage systems. Renewable Energy 2019; 133: 190-204.

[19] M.Cascetta, F. Serra, G.Cau, P.Puddu. Comparison between experimental and numerical results of a packed-bed thermal energy storage system in continuous operation. Energy Procedia 2018; 148:234-241.
[20] T. Esence, A. Bruch, S. Molina, B. Stutz, J.F. Fourmigue. A review on experience feedback and numerical modeling of packed-bed thermal energy storage systems. Solar Energy 2017; 153: 628-654.
[21] R. Anderson, L. Bates, E. Johnson, J.F. Morris. Packed bed thermal energy storage: A simplified experimentally validated model. Journal of Energy Storage 2015; 4: 14–23.
[22] H. Agalit, N. Zari, M. Maalmi, M. Maaroufi. Numerical investigations of high temperature packed bed TES systems used in hybrid solar tower power plants. Solar Energy 2015; 122: 603–616.
[23] F. Opitz, P. Treffinger. Packed bed thermal energy storage model– Generalized approach and experimental validation. Appl Therm Eng 2014; 73:245-252.
[24] P. Klein, T.H. Roos, T.J. Sheer. Experimental investigation into a packed bed thermal storage solution for solar gas turbine systems. Energy Procedia 2014; 49: 840 – 849.
[25] H. Bindra, P. Bueno, J.F. Morris, R. Shinnar. Thermal analysis and exergy evaluation of packed bed thermal storage systems. Applied Thermal Engineering 2013; 52: 255-263.
[26] M. Hänchen, S. Brückner, A. Steinfeld. High-temperature thermal storage using a packed bed of rocks- Heat transfer analysis and experimental validation. Appl Therm Eng 2011; 31:1798-1806.
[27] A.J. White. Loss analysis of thermal reservoirs for electrical energy storage schemes. Applied Energy 2011; 88: 4150-4159.
[28] J. Marti, L. Geissbühler, V. Becattini, A. Haselbacher, A. Steinfeld. Constrained multi-objective optimization of thermocline packed-bed thermal-energy storage. Applied Energy 2018; 216: 694–708.
[29] J.D. McTigue, C.N. Markides, A.J. White. Performance response of packed-bed thermal storage to cycle duration perturbations. Journal of Energy Storage 2018; 19:379–392.
[30] J.D. McTigue, A.J. White. A comparison of radial-flow and axial-flow packed beds for thermal energy storage. Applied Energy 2018; 227: 533–541.
[31] I. Ortega-Fernández, I. Loroño, A. Faik, I. Uriz, J. Rodríguez-Aseguinolaza, B. D'Aguanno. Parametric analysis of a packed bed thermal energy storage system. AIP Conference Proceedings 2017; 1850 080021. https://doi.org/10.1063/1.4984442
[32] A.J. White, J.D. McTigue, C.N. Markides. Analysis and optimisation of packed-bed thermal reservoirs for electricity storage applications. Proc IMechE Part A: J Power and Energy 2016; 230:739-754.
[33] G. Zanganeh, A. Pedretti, A. Haselbacher, A. Steinfeld. Design of packed bed thermal energy storage systems for high-temperature industrial process heat. Applied Energy 2015; 137: 812–822.
[34] P. Klein, T.H. Roos, T.J. Sheer. Parametric analysis of a high temperature packed bed thermal storage design for a solar gas turbine. Solar Energy 2015; 118:59–73.
[35] H. Bindra, P. Bueno, J.F. Morris. Sliding flow method for exergetically efficient packed bed thermal storage. Applied Thermal Engineering 2014; 64: 201-208.
[36] N.Mertens, F.Alobaid,L.Frigge,B.Epple. Dynamic simulation of integrated rock-bed thermocline storage for concentrated solar power. Solar Energy. 2014; 110:830-842.
[37] G. Zanganeh, A. Pedretti, S. Zavattoni, M. Barbato, A. Steinfeld. Packed-bed thermal storage for concentrated solar power – Pilot-scale demonstration and industrial-scale design. Solar Energy 2012; 86:3084-98.
[38] B. Cardenas, T.R. Davenne, J.P. Rouse, S.D. Garvey. Effect of design parameters on the exergy efficiency of a utility-scale packed bed. Journal of Energy Storage 2018; 18: 267–284.
[39] B. Cardenas, T. Davenne, J. Wang, Y. Ding, Y. Jin, H. Chen, Y. Wu, S. Garvey. Techno-economic optimization of a packed-bed for utility-scale energy storage. Applied Thermal Engineering. In Press.
[40] T.R. Davenne, S.D. Garvey, B. Cardenas, M.C. Simpson. The cold store for a pumped thermal energy storage system. Journal of Energy Storage 2017; 14: 295–310.
[41] B. Cardenas, T.R.Davenne, S.Garvey. A sign-preserving filter for signal decomposition. Proc IMechE Part I: J Systems and Control Engineering 2018; 1-21. DOI: 10.1177/0959651818811182
[42] B. Cardenas, S.D. Garvey. Load optimization for reducing the cost of an electric vehicle's battery pack. Journal of Energy Storage 2018; 20: 254–263.
[43] M. Medrano, A. Gil, I. Martorell, X. Potau, L.F. Cabeza. State of the art on high-temperature thermal energy storage for power generation. Part 2: Case studies Renewable and Sustainable Energy Reviews 2010; 14: 56–72.
[44] S.Zunft. Adiabatic CAES: The ADELE-ING project. Presented in: SCCER Heat & Electricity Storage Symposium. Villigen, Switzerland, May, 2015.
[45] P. Hartlieb, M. Toifl, F. Kuchar, R. Meisels, T. Antretter. Thermo-physical properties of selected hard rocks and their relation to microwave assisted comminution. Minerals Engineering 2016; 91:34-41
[46] E.W. Lemmon, R.T. Jacobsen. Viscosity and thermal conductivity equations for nitrogen, oxygen, argon and air, Int. J.Thermophys. 2004; 25:21–69.
[47] E.W. Lemmon, R.T. Jacobsen, S.G. Penoncello, D.G. Friend. Thermodynamic properties of air and mixtures of nitrogen, argon and oxygen from 60 to 2000 K at pressures to 2000 MPa, J. Phys. Chem. Ref. Data 2000; 29: 331–385.
[48] A. Felix Regin, S.C. Solanki, J.S. Saini. An analysis of a packed bed latent heat thermal energy storage system using PCM capsules: Numerical investigation. Renewable energy 2009; 34:1765-1773.
[49] K.G. Allen, T.W. Backström, D.G. Kröger. Rock bed pressure drop and heat transfer: Simple design correlations. Solar energy 2015; 115:525-536
[50] K.G. Allen, T.W. Backström, D.G. Kröger. Packed rock bed thermal storage in power plants: design considerations. Energy Procedia 2014; 49:666-675
[51] S. Ergun. Fluid flow through paced columns. Chemical Engineering Progress 1952; 48:89-94.
[52] M. Cascetta, G. Cau, P. Puddu, F. Serra. A study of a packed bed thermal Energy Storage device: test rig, experimental and numerical results. Energy Procedia 2015; 81:987-994
[53] I. Ortega-Fernández, J. Rodríguez-Aseguinolaza. Thermal energy storage for waste heat recovery in the steelworks: The case study of the REslag project. Applied Energy 2019; 237: 708-719
[54] B. Cárdenas, A.J. Pimm, B. Kantharaj, M.C. Simpson, J.A. Garvey, S.D. Garvey. Lowering the cost of large-scale energy storage: High temperature adiabatic compressed air energy storage. Propulsion and Power Research 2017; 6(2):126–133.